2D materials beyond graphene for high-performance energy storage applications

Xiaoyan Zhang, Lili Hou, Artur Ciesielski and Paolo Samorì*

ISIS & icFRC, Université de Strasbourg & CNRS, 8 allée Gaspard Monge, 67000 Strasbourg, France
Email: samori@unistra.fr

Energy crisis is one of the most urgent and critical issues in our modern society. Currently, there is an increasing demand for efficient, low-cost, light-weight, flexible and environmentally benign, small-, medium-, and large-scale energy storage devices, which can be used to power smart grids, portable electronic devices, and electric vehicles. Novel electrode materials, with a high energy density at high power are urgently needed for realizing high-performance energy storage devices. The recent development in the field of 2D materials, including both graphene and other layered systems, has shown promise for a wide range of applications. In particular, graphene analogues, due to their remarkable electrochemical properties, have shown great potential in energy-related applications. This review aims at providing an overview of current research and important advances on the development of 2D materials beyond graphene for supercapacitors and batteries. The major challenges to be tackled, and more generally the future directions in the field, are also highlighted.

1. Introduction

The exhaustion of fossils fuels and climate change are among the greatest problems faced by our modern society. To counteract the growing energy consumption demand, there is an urgent need to design sustainable, efficient and low-cost devices for energy production and storage. Being confronted with the colossal energy requirements against the backdrop of global warming and the looming energy crisis, the development of clean and renewable energy materials as well as their devices is highly desirable. Harnessing renewable energy sources such as sunlight or wind is a first consideration for sustainable energy production. However, they are diffuse and intermittent, owing to the unreliability of nature. Conversely, tidal power and wave energy rely on a constant flow thus are more predictable and abundant, yet, likewise geothermal energy, they can only be produced at selected sites; the collection of the generated energy and its transmission is unfortunately a big hurdle towards these technologies. These drawbacks have stimulated the research on efficient energy storage devices featuring high-energy capacity and excellent cycle performance. Energy storage devices such as supercapacitors and batteries, with high power/energy densities, are expected to play essential roles in our daily life as the dominant power sources for portable consumer electronics (e.g., smartphones, tablets, notebook PCs and camcorders), hybrid electric/plug-in-hybrid vehicles and smart grids.[1-6]

The recently increased research efforts on 2D materials, *i.e.*, graphene and its analogues, is to a great extent the result of the promise that they hold for technological applications including electronic devices, sensors, catalysts, energy conversion and storage devices, *etc*., by taking full advantage of their outstanding electrical, optical, chemical, and thermal properties.[7-14] Beyond graphene, other layered materials possessing various elemental compositions and different crystallographic structures, offer a broad portfolio of material's solutions with tunable chemical and physical properties for application as high-performance active components, which can operate as electrode materials for high-performance electrochemical

energy storage devices.[4, 15, 16] Although graphene-based nanomaterials have demonstrated outstanding performance as electrodes in energy storage devices, new alternative nanomaterials should also be developed in order to further improve the electrochemical performance. Other 2D materials as graphene analogues (GAs) are expected to have broad implications in next generation of clean, efficient, and renewable energy systems. Layered materials of GAs refer to layered materials having similar structure as graphene, with planar topology and ultrathin thickness (single to few atomic layers). Typical GAs for energy storage include transition metal dichalcogenides (TMDs), transition metal oxides (TMOs)/hydroxides (TMHs), metal sulfides, phosphorenes, MXenes, silicences, *etc* (**Figure 1**).[17]

Insert **Figure 1** here

Due to their thickness on the atomic scale, their inherent properties differ from those of their bulk lamellar systems. In particular, the quantum confinement of electrons in the 2D plane imparts them with unprecedented electrical and electronic characteristics (**Table 1**).[18-26] Moreover, it is well known that the delivered specific capacity of electrode materials is closely related with the reaction kinetics during the charging/discharging process.[3] In view of their high surface-to-volume ratio, GAs offer high specific surface areas (**Table 1**) to enable full utilization of all available sites of active electrode materials.[27-30] As a result, the exposed contact area is significantly enhanced between the electrodes and electrolytes, and also the paths for transport of charges are largely shortened. Last but not least, GAs also exhibit excellent electrochemical properties.[31] All of these characteristics make them potential candidates for energy storage devices.

Insert **Table 1** here

In this contribution, after a brief introduction on the preparation methods of GAs, we review the most enlightening recent progresses of GAs in energy storage devices, providing outlooks and perspectives of this topical area of science and technology.

2. Preparation methods of GAs

Since there are already several excellent review articles discussing the unique properties of layered materials beyond graphene,[32-37] in the present review we will not focus on their properties. Prior to discussing applications in supercapacitors and batteries, we briefly introduce the methods for the preparation of GAs. The reliable production of high-quality atomically thin 2D systems and the fine-tuning of their various properties through scalable approaches is a crucial first step for realizing devices for energy storage. Hitherto, two approaches have been pursued to obtain monolayer-thick GAs sheets, *i.e.*, the *top-down* and *bottom-up* strategies (**Figure 2**). The former relies on the chemical[38] or mechanical[39-41] exfoliation of bulk crystals into individual sheets; the latter allows the generation of GAs from atoms or suitably designed molecular building blocks, which upon chemical reactions form covalently linked GAs sheets.[42]

Insert **Figure 2** here

2.1 *Top-down* approaches

The *top-down* approaches enable the production of micrometer- and/or nanometer-sized sheets from bulk crystals. On the one hand, it is generally assumed that the GAs sheets produced *via* mechanical cleavage (scotch tape method) possess highest quality and purity, which makes them suitable for fundamental research, and in particular for realization of proof-of-concept devices.[43] Yet, mechanical cleavage is unsuitable for mass production due to the low yield and lack of control over the number of layers in the exfoliated samples. On the other hand, large quantities of mono- and few-layer thick GAs sheets, characterized by a low content of structural defects, can be obtained by exploring *top-down* methods such as ultrasound-induced liquid-phase exfoliation (UILPE)[44-47] or electrochemical liquid-phase exfoliation (ELPE),[48-52] which are extremely versatile and can be carried out in a variety of environments. Other methods, which combine intercalation of bulk crystals with chemical inserts and its subsequent exfoliation, are also being developed.[53]

2.2 *Bottom-up* approaches

The *bottom-up* production of large-area GAs with specific number of layers can be achieved by making use of chemical vapor deposition (CVD) techniques.[54] Among the CVD methods, sulfurization (or selenization) of metal (or metal oxide) thin films is being extensively explored.[55, 56] Another useful method is to synthesize 2D materials using molecular precursors *via* a wet chemical hydrothermal/solvothermal treatment. For instance, GAs like TMOs can be produced *via* self-assembly, where amphiphilic block copolymers and short-chain alcohol co-surfactants are employed as structure-directing agents to confine the stacking and growth of the metal oxide precursor oligomers along the chosen direction.[57]

As for energy storage, UILPE[39, 44-46] and wet chemical synthesis[57] are the most commonly used approaches for the preparation of layered materials of GAs, owing to the advantages discussed above as well as of easy and large-scale preparation.

3. Supercapacitors

Supercapacitors, also named as electrochemical capacitors, have attracted tremendous research interest during the past decades, primarily due to their high power density, rapid charging/discharging, and excellent cycle stability.[2] Undoubtedly, supercapacitors provide a promising approach to resolve the current energy demand by allowing fast storage of intermittent renewable energy. Based on the underlying energy storage mechanism, supercapacitors can be divided into two types: electrical double-layer capacitors and pseudocapacitors.[58] The performance of supercapacitors can be evaluated by using the following parameters: i) mass/volume capacitance, ii) energy/power density, and iii) cycle lifetime. The unique characteristics that make a material suitable as an active electrode include good electrical conductivity, high specific surface area, optimized pore size

distribution, as well as proper introduction of doping, which determine the final performance of supercapacitors.[59] Moreover, other factors like the choice of electrode configuration, electrolytes, mass loading, voltage applied, *etc*., also play an important role in the outcome of supercapacitors.[3] The progress in supercapacitor technologies can surely benefit from the development of novel nanostructured electrode materials.[59] Presently, intensive research efforts on supercapacitors are devoted towards developing/discovering new electrode materials with enhanced energy storage capability and a long cycle life, meanwhile reducing cost to realize their extensive usage in our daily life.

3.1 Electrical double-layer capacitors

In electrical double-layer capacitors (EDLCs), the capacitance arises from the adsorption of both positive and negative ions in a double layer at the electrode/electrolyte interface; therefore, it is highly dependent on the specific surface area of the electrode materials that is accessible to electrolyte ions. During the charging process, negative ions move to the positive electrode, while positive ions transfer towards the negative electrode (**Figure 3**). The direction of ions movement is reversed in the discharging process.[58] Typically, the electrodes used in EDLCs are composed of porous carbon-based materials,[60, 61] including activated carbon,[62] mesoporous carbon,[63] carbon nanofibers,[64] carbon nanotubes,[65] graphene,[66] and carbide-derived carbons.[67]

Insert **Figure 3** here

GAs with high electric conductivity would be of high interest and of significance for fabrication of supercapacitors. However, semiconducting GAs such as MoS_2 or WS_2 possess relatively low electrical conductivities,[68, 69] which hampers their use as electrodes in supercapacitors. To overcome this problem, Chhowalla and co-workers reported an approach to prepare chemically exfoliated sheets of MoS_2 using organolithium compounds with a high concentration of the metallic 1T (stands for a trigonal unit cell consisting of single-layer)

phase.[70] The metallic MoS_2 sheets with electrical conductivity values of 10^3 to 10^4 S m^{-1}, can be electrochemically intercalated by ions such as H$^+$, Li$^+$, Na$^+$ and K$^+$ with very high efficiency. The as-fabricated supercapacitors without binders and other additives can achieve specific volume capacitance values ranging from ~400 to ~700 F cm^{-3} in a variety of aqueous electrolytes. In addition, they also showed that 1T MoS_2 is suitable for high-voltage (3.5 V) operation in organic electrolytes (**Figure 4, a-c**), with high volumetric energy and power density values, coulombic efficiencies in excess of 95%, and good stability over 5,000 cycles. As evidenced by X-ray diffraction analysis, these favourable electrochemical properties of 1T MoS_2 sheets are mainly the result of their hydrophilic nature and high electrical conductivity, as well as the ability of the exfoliated layers to dynamically expand and intercalate the various ions. It is known that the transition metal of Mo center can exhibit oxidation states from +2 to +6, rendering it pseudocapacitive abilities like RuO_2. In this case, besides EDLCs, there is also some contribution from charge transfer (pseudocapacitance), as evidenced by Nyquist plots. In another study, Bissett *et al*. prepared MoS_2/graphene nanocomposites, used them as active materials in supercapacitors and they observed a transition from EDLCs to pseudocapacitance in the charge storage mechanism.[71] Tour and co-workers attributed the storage mechanism of MoS_2 nanoporous films as a combination of both EDLCs and pseudocapacitance.[72] Soon and Loh pointed out that besides double-layer capacitance, diffusion of the ions into the MoS_2 films at slow scan rates gives rise to faradaic capacitance, which enhances the capacitance significantly.[73] However, the exact storage mechanism of MoS_2 requires a further in-depth studies in order to be fully unravelled.

Insert **Figure 4** here

As alternative, another member of the TMD family such as vanadium disulfide (VS_2) has been also exploited. VS_2 crystals are composed of the metal V layers sandwiched between two sulfur layers and stacked together by weak van der Waals interactions. VS_2 is one of the TMDs which has been only recently explored: it possesses metallic electrical behaviour,

rendering it interesting for application as high-performance electrodes for supercapacitors. In a recent study, Xie and co-workers developed a unique ammonia-assisted chemical strategy to exfoliate bulk VS_2 flakes into ultrathin metallic VS_2 sheets of less than five layers, which can be assembled into thin films *via* a vacuum filtration process and further used as electrode active materials to construct planar supercapacitors (**Figure 4, d-f**).[74] The highly conductive VS_2 thin film not only prompts ion transport during the charge/discharge process, but also brings a small series resistance inside the electrodes. The cyclic voltammetry (CV) curves showed near-rectangular shapes at different scan rates and no obvious redox peaks were observed, attributed to typical double-layer capacitor behaviors by the authors. However, in this case, the contribution from pseudocapacitance cannot be totally ruled out since rectangular CV curves are not only related to EDLCs (MnO_2 also shows rectangular CV curves, but is a typical pseudocapacitive electrode material). In-situ X-ray absorption spectroscopy (XAS) or other techniques that allow monitoring changes in the valence state of elements are needed to find out the exact storage mechanism. Importantly, the as-fabricated VS_2 in-plane supercapacitors displayeds a specific capacitance as high as 4760 μF cm^{-2} with no obvious degradation after 1000 charge/discharge cycles, thereby opening the door to the design of in-plane supercapacitors with high performance based on layered materials for the practical power sources in advanced intelligent devices.

3.2 Pseudocapacitors

In contrast to EDLCs, pseudocapacitors store energy through fast and reversible faradaic redox reactions with charge transfer occurring at or near the electrode surface (**Figure 5**).[58] Pseudocapacitive electrode materials, with reversibly faradic reaction behaviour, are of great research interests. The amount of electric charge stored in pseudocapacitors is linearly proportional to the applied voltage. When an external potential is applied, the active electrode materials undergo reversible redox reactions, generating charges and resulting in faradaic

current passing through the cell of supercapacitors. Since the specific capacitance depends on the faradaic charges generated at or near the electrode surface, it is very important to use pseudocapacitive electrode materials with high charge generation and storage ability in a short period of time. The most widely used pseudocapacitive electrode materials include conducting polymers[75] and TMOs/TMHs.[76-78] Pseudocapacitors can achieve much higher energy densities than EDLCs (10 to 100 times), since they can provide a variety of oxidation states for efficient redox charge transfer reactions between electrodes and adsorbed/inserted electrolyte ions.

Insert **Figure 5** here

Among various materials used as electrodes for pseudocapacitors, TMOs and TMHs have been widely employed due to their large theoretical capacity,[76-79] chemical stability and compatibility with electrolytes, as well as their facile preparation, which are vital to achieve durable and cost-effective energy storage. The electrochemically redox active transition metal layered materials usually possess high specific capacitances, which are favourable for high energy density storage. For example, Zhang *et al.* prepared thin 2D sheets of $Co_3V_2O_8$ *via* a hydrothermal approach and the as-synthesized sheets were used as an active electrode material in supercapacitors.[77] The assembled device showed a specific capacitance of 739 F g^{-1}, with a cycle stability of 95.3% after 2000 cycles at 0.5 A g^{-1}. In another case, Xie's group synthesized single layer β-Co(OH)$_2$ with five-atoms layer thickness through a facile oriented-attachment strategy.[78] An all-solid-state asymmetric supercapacitor fabricated from using single-layer β-Co(OH)$_2$ as cathode and nitrogen-doped graphene as anode, exhibited a high energy density of 98.9 Wh kg^{-1} at a power density of 17981 W kg^{-1}, and also excellent cycling life with 93.2% capacity retention after 10 000 charge/discharge cycles.

Insert **Figure 6** here

For energy storage devices, highly conductive active electrode materials are required to realize fast charge diffusion, leading to quick electrical responses and low resistance loss.

Therefore, it is crucial to control/optimize the electrical conductivity of the active electrodes in order to achieve high specific capacitance and rate capability. As a typical example, conductive MXenes have been employed as electrode materials for pseudocapacitors, demonstrating a very high volumetric capacitance.[80-83] Gogotsi and co-workers demonstrated a facile strategy for the *in situ* polymerization of pyrrole confined between conductive $Ti_3C_2T_x$ layers.[82] Polypyrrole (PPy), as a conductive polymer, can intercalate between the $Ti_3C_2T_x$ layers increasing the space for rapid charge transport, and can also provide conductive aligned paths for charge percolation. When tested as supercapacitor electrodes, the $PPy/Ti_3C_2T_x$ composite displayed a volumetric capacitance of ≈ 1000 F cm^{-3} with capacitance retention of 92% after 25000 cycles (**Figure 6**), indicating high electrochemical performance and excellent cycle life. The enhanced capacitance is due to the synergistic effect between the $Ti_3C_2T_x$ layers and the conductive PPy. The strategy can be used to synthesize other conducting polymer/MXene composites for energy-related application. However, in practice, the low electrical conductivity of most GAs (such as TMOs, TMHs, and TMDs) limits the ion diffusion rate in those electrode materials. As a consequence, their redox reversibility could be affected, notably rendering them inappropriate for high-rate energy storage devices. To solve the problem, combination of GAs with other conductive materials, including graphene,[84-87] carbon nanotubes,[88-90] carbon nanofibres,[91] metals,[92] conducting polymers,[93-96] conductive substrates,[97-100] *etc.*, has been investigated to enhance the overall performance of supercapacitors based on GAs, by taking the advantage of the high conductivity of the conductive scaffolds. Moreover, these strategies may allow more electrolyte ions to penetrate efficiently into the hybrid electrode materials during charging/discharging processes. A remarkable example has been reported by Chang *et al.* by fabricating asymmetric supercapacitors based on reduced graphene oxide (RGO)/MnO_2 as the anode and RGO/MoO_3 as the cathode.[85] For the anode, mesoporous MnO_2 nanospheres exhibit short diffusion path length for both ions of electrolyte and electrons, favouring

10

migration of ions during rapid charging/discharging process. For the cathode, the thin MoO_3 sheets support short diffusion path length for ions of electrolyte in the perpendicular direction and continuous transport pathways for electrons in the parallel direction. The introduction of graphene into the two active electrodes further offers extra interface at the hybridized interlayer areas to facilitate charge transport during charging/discharging processes, improving the pseudocapacitive reactions and rate capability. The devices showed a high energy density of 42.6 Wh kg^{-1} at a power density of 276 W kg^{-1} and a maximum specific capacitance of 307 F g^{-1}. Remarkably, the specific capacitance was improved even after 10000 cycles, which is attributed to the development of micropore structures during the repetition of ion transfer.

Insert **Figure 7** here

Light-weight, flexible energy storage devices are highly desirable for portable flexible electronics. Feng *et al*. fabricated cellulose paper (CP)-based asymmetrical, flexible thin film supercapacitors using graphite/Ni/Co_2NiO_4 sheets-CP as positive electrode and graphite/Ni/active carbon-CP as negative electrode (**Figure 7**).[101] The assembled device shows a high volumetric energy density (2.48 mWh cm^{-3}, 80 Wh kg^{-1}), a high volumetric power density (0.79 W cm^{-3}, 25.6 kW kg^{-1}) and an excellent cycle stability at different bending states (< 4% capacitance loss after 20 000 cycles). This study gives a good example of design and fabrication of high performance and flexible energy storage devices.

Besides coupling GAs with conductive nanomaterials, other strategies have also been pursued in order to improve the electrical conductivity of the former. For instance, Wang *et al*. synthesized nickel-cobalt-aluminium layered hydroxides and further chemically treated them with sodium hydroxide yielding enhanced electrical conductivity, which is caused by partial conversion of Co^{2+} to a more conductive Co^{3+} state.[102] The obtained layered hydroxides show a high specific capacitance of 738 F g^{-1} at 30 A g^{-1}, which is 57.2% of 1289 F g^{-1} at 1 A g^{-1}.

Insert **Table 2** here

As electrode materials for supercapacitors, GAs possess obvious advantages, such as high specific surface areas for ion adsorption, open 2D channels for ion transport, and also large theoretical capacity. However, the low electrical conductivity of GAs limits ion diffusion rates and induces a high resistance loss.

4. Batteries

Due to their combination of apparent high surface-to-volume ratio and excellent electrochemical properties, layered materials are also promising candidates for electrodes to be used in batteries. Remarkable progress has been made using GAs in lithium-ion batteries (LIBs), sodium-ion batteries (SIBs), lithium-sulphur (Li-S) batteries and other kinds of batteries. Here we will mainly discuss their applications in LIBs and SIBs.

4.1 Lithium-ion batteries

Lithium-ion batteries (LIBs) have been developed quite rapidly since their first commercialization by Sony in 1991, and have become one of the most popular rechargeable batteries with many outstanding features including high energy density, low maintenance, no memory effect, and little self-discharge (only a slow loss of capacity when not in use).[103] LIBs are used as the dominant power source for many portable electronic devices (e.g., cell phones, laptops, digital cameras, *etc*.), and they are expected to hold great potential for the upcoming large-scale applications (e.g., electric cars and stationary energy backup systems). For LIBs, the electrochemical reaction of lithium ions is realized through different chemical pathways, such as *via* an intercalation/de-intercalation reaction, conversion reaction and alloying/de-alloying reaction.[103]

The working principle of a conventional LIB cell is based on the reversible shuttling of lithium ions, which results in a difference of electrochemical properties between the anode

12

and the cathode.[103] Therefore, the inherent properties of the electrode materials represent a key factor largely affecting the overall performance of LIBs. Hitherto, graphite is still the most widely employed anode material for LIBs due to its flat potential profile, high columbic efficiency, and good cycling performance.[104] However, graphite itself possesses a relatively low theoretical capacity (372 mAh g^{-1}). Furthermore, the slow Li ions diffusion rate of 10^{-8} cm^2 s^{-1} in the graphite structure results in a low power density of LIBs. Thus, there is a need to develop new electrode materials for LIBs. Tremendous efforts are being made to explore alternative anode materials with a higher lithium storage capacity, better rate capability and cycle stability. Numerous candidates including graphene,[105, 106] metals,[107] and metal oxides[108] have been investigated, trying to address these challenges. Among them, sheets of GAs have been considered as promising electrode candidates for LIBs to offer the advantages of a larger capacity over traditional graphite anode. Generally speaking, lithium storage based on layered materials benefits from the structural qualities of these nanoscale systems such as their high surface area, large void space and good structural stability.

Insert **Figure 8** here

Sheets of TMOs have been widely exploited as components for LIBs also because they exhibit some advantages such as high specific capacity, good stability, widespread availability, relatively easy to prepare and their environmental friendly nature. Lithium storage in these electrode materials is based on the reversible redox reaction between lithium and transition metal cations, which is termed as "conversion reaction".[109] TMOs such as Fe_2O_3,[110, 111] V_2O_5,[112] Nb_2O_5[113] and TiO_2[114-116] have been used as anodes in LIBs. Fe_2O_3, as a typical TMOs, because of its very high theoretical specific capacity of 1006 mAh g^{-1}, it has been considered as a very promising candidate for the next generation of anode materials in batteries. Cao et $al.$ fabricated 3D hierarchical porous α-Fe_2O_3 sheets on copper foil using hydrothermal and annealing treatments, and then directly used as a binder-free anode for LIBs (**Figure 8**).[110] A good capacity of 433 mA h g^{-1} is retained at a high current of 20.1 A g^{-1},

and a reversible capacity up to 877.7 mAh g^{-1} is maintained after 1000 cycles at 2.01 A g^{-1}, demonstrating a high reversible capability and outstanding rate performance. The unique porous 3D hierarchical nanostructure enhances the electrochemical performance not only by facilitating the kinetics for Li ions diffusion by shortening the diffusion pathways to the nanoscale due to the large electrode–electrolyte contact area, but also by improving the electrode stability because of the reduced lattice strain associated with lithium intercalation. Moreover, the 3D conductive network based on the conversion reaction mechanism (Fe_2O_3 + $6Li \leftrightarrow 2Fe$ + $3Li_2O$) is formed during cycling, guaranteeing efficient electron transportation. The *in-situ* fabricated free-standing and aligned 3D hierarchical nanostructure ensures good electronic contact between the α-Fe_2O_3 sheets and the Cu current collector, which theoretically facilitates electrons flow between the substrate and α-Fe_2O_3 flakes. However, in this case, a very low mass loading (0.35 mg cm^{-2}) is used, which might be related with the low tap/packing density of the 3D hierarchical porous α-Fe_2O_3 sheets. The use of low mass loading of nanostructured materials leads to devices with moderate performance and limited cycle life.[1] For reliable measurements and practical applications, test cells should have active materials with mass loadings on the order of 10 mg cm^{-2}. For 2D structure of TiO_2, its ease of structural tailoring, its low volume expansion upon lithiation combined with good stability and lack of lithium plating endow this layered material a great potential to be charged/discharged at high current rates for extended cycling.[114-116]

Insert **Figure 9** here

Superior to single-phase oxides, the strongly coupled mixed-metal oxides may synergistically enhance the electrochemical properties such as reversible capacity, electrical/ionic conductivity, and also mechanical stability, leading to better electrochemical performance.[117-121] Wang and co-workers reported a method to prepare $Co_3V_2O_8$ sheets *via* a simple hydrothermal method followed by annealing.[117] The sheets based electrodes exhibit outstanding reversible capacity (1114 mA h g^{-1} retained after 100 cycles) and excellent rate

performance (361 mA h g^{-1} at a high current density of 10 A g^{-1}) for lithium storage (**Figure 9**). Detailed studies of the morphological and structural changes of Co$_3$V$_2$O$_8$ upon cycling indicate that reversible conversion reactions between Co and CoO are proceeding on the amorphous lithiated vanadium oxides matrixes. The excellent electrochemical performances of the multilayer Co$_3$V$_2$O$_8$ are attributed to the unique morphologies and especially to the surface-to-surface constructions generated during the lithium ion insertion processes. However, it should be mentioned that the first change/discharge cycle shows a low Coulombic efficiency (a high first cycle irreversible capacity loss), due to deconstruction of the Co$_3$V$_2$O$_8$ sheets, formation of amorphous Li$_x$V$_2$O$_5$ and also possible formation of solid electrolyte interface (SEI). This phenomenon has also been observed in other 2D sheets,[122] which can be suppressed through surface modification.[123]

Besides TMOs, TMDs,[124-126] transition metal trichalcogenides (TMTs),[127] and phosphorenes,[128] other layered materials like transition metal carbides (also named as MXenes) have also been employed as electrodes in LIBs.[129, 130] Naguib *et al.* synthesized 2D niobium and vanadium carbides by selective etching of Nb$_2$AlC and V$_2$AlC powders in concentrated HF solutions at room temperature, yielding Nb$_2$CT$_x$ and V$_2$CT$_x$, respectively.[130] When tested as electrodes in LIBs, reversible capacities of 170 and 260 mAh g^{-1} at 1 C, and 110 and 125 mAh g^{-1} at a high rate of 10 C were obtained after 150 cycles for Nb$_2$CT$_x$ or V$_2$CT$_x$, respectively, suggesting fast Li diffusion between MXene layers and potential use in high power applications.

Insert **Figure 10** here

As already discussed in the *Section 3*, single component 2D materials may not meet all the requirements for high rate energy storage devices. Their high reaction activity endows them with relatively good electrochemical performance, however the relatively low conductivity hampers their efficiency.[110-120, 124] For example, metal oxide anodes usually possess low rate capability and poor cycling stability owing to inherently poor electronic conductivity, slow

reaction kinetics, and severe volume expansion during discharge–charge cycles.[110-120] Therefore, rationally introducing *ad hoc* functional nanomaterials into single component 2D system may be a route to improve the performance of energy storage devices in terms of capacity, efficiency, activity, and stability, which may origin from the synergetic effect. Layered materials such as TMOs, TMDs, phosphorenes, metal carbides, metal sulfides or silicenes can be combined with RGO/graphene,[131-149] doped RGO/graphene,[150-153] CNT,[154-158] conductive carbon,[159-168] carbon nanofibers,[169] carbon nanoboxes,[170] metals,[171] or conducting polymers,[172] generating hybrid electrode materials for LIBs with excellent performance. Dou and co-workers fabricated an atomic layer-by-layer structure of Co_3O_4/graphene and used it as an anode for LIBs.[131] This delicate nanostructure shows very high specific capacities of 2014.7 and 1134.4 mAh g^{-1} at 0.11 and 2.25 C, respectively, indicating excellent rate capability, and also exhibits ultralong cycle life up to 2000 cycles without obvious capacity fading at 2.25 C. MoS_2, when used as electrodes for LIBs, still suffers from fast structural deterioration during lithiation/delithiation process and poor electrical conductivity, resulting in pulverization, thus unsatisfactory cycling performance and rate capability. Wang *et al.* designed a new, robust nanocomposite based on MoS_2 and S-doped RGO through a facile solvothermal approach combined with annealing, and the hybrid is then used as an anode for LIBs (**Figure 10**).[152] The MoS_2 sheets are covalently bridged to S-doped RGO, which is confirmed by X-ray photoelectron spectroscopy (XPS) and density functional theory (DFT) calculations. The intimate contact between the two components guarantees efficient electron transfer pathways. Such a composite shows a superior rate capability of 915 mAh g^{-1} at 10 A g^{-1}, and exhibits a long cycle stability with a capacity of 92.3% retained after 2000 cycles at 10 A g^{-1}. In another example, Yu and co-workers synthesized carbon nanofibers decorated with MoS_2 sheets (CNFs@MoS_2) through a solution coating and a subsequent annealing process.[169] The CNFs@MoS_2 nanofibers show excellent Li storage properties with a high specific capacity (1489 mAh g^{-1} upon initial discharge), an

excellent cycling performance (1264 mAh g^{-1} after 50 cycles) and a good rate performance (860 mAh g^{-1} at 5 A g^{-1}), making it a promising anode material for high-energy LIBs (**Figure 11**). The synergistic effect between the two components facilitates the formation of a hierarchically conductive network with much improved electrode kinetics and cycling stability.

Insert **Figure 11** here

Other materials like Si also have some drawbacks when exploited as components in electrodes for LIBs, such as their poor electrical conductivity, their large volume change during the lithiation−delithiation process, and serious degradation from unstable solid electrolyte interphase (SEI) layers. Park's group prepared carbon-coated Si sheets *via* one-step simultaneous molten salt-induced exfoliation and chemical reduction process, and further coated by carbon layers through thermal decomposition in an acetylene atmosphere.[162] The as-fabricated anode shows a high reversible capacity (865 mAh g^{-1} at 1.0 A g^{-1}), an outstanding capacity retention (92.3% after 500 cycles at 0.5 C), an excellent rate capability (a capacity of 60% at 20 C compared to 2 C), and remarkably suppressed volume expansion (42% after 200 cycles at a rate of 0.2 C). All the above discussed strategies can be easily applied/extended to design other novel nanocomposites based on GAs/conductive fillers, which hold great promise in next-generation rechargeable LIBs.

4.2 Sodium-ion batteries

As lithium resources are relatively expensive and geographically constrained, developing new type of batteries with a high electrochemical performance while a lower cost is highly desirable. Sodium is the second-lightest and -smallest alkali metal next to lithium, and they share common physico-chemical properties. The abundance and low cost of sodium in the earth and its low redox potential (slightly higher than lithium) promote sodium-ion batteries (SIBs) as a promising alternative to LIBs for electric vehicles and grid-level energy storage.

The energy density for SIBs is expected to be above 200 Wh Kg^{-1}. SIBs have a similar operation mechanism as LIBs, which potentially provides high reversibility and long cycling life. During charging process, an oxidation reaction occurs at the cathode with Na de-insertion and electron loss. The sodium ions move to the anode *via* the electrolyte, and electrons simultaneously transfer to the anode through external conduction path. This leads to a reduction reaction occurring at the anode with Na insertion. An opposite process occurs during the discharging process. Currently, the low capacity, poor rate capability, and cycling stability of existing anodes significantly hinder the practical applications of SIBs. One major scientific issue for a competitive SIBs technology is to develop viable electrode materials with a high specific capacity and appropriately low redox potentials.

Compared to LIBs, the larger size of sodium ions (1.02 Å vs. 0.76 Å for lithium ions) hampers the kinetics of electrochemical reactions. Therefore, reversible electrode materials are required to possess large enough channels and/or interstitial sites. Nowadays, layered TMOs and TMDs (such as MoS$_2$ and SnS$_2$) have been employed as electrode materials in SIBs.[173-177] The large interlayer distance in TMDs is beneficial to the accommodation of sodium ions. However, due to their low electrical conductivity, the overall performance especially the high-rate capability (kinetic factors such as ion diffusivity and electron conductivity) is still far beyond satisfaction. For example, Wang and co-workers reported a liquid phase exfoliation approach to prepare few-layer thick MoS$_2$ inks and used them as an anode material in SIBs.[176] The MoS$_2$ based electrode only showed a moderate capacity of 530 mAh g^{-1} at 40 mA g^{-1}. Therefore, introducing foreign counterparts with good conductivity holds the potential to solve the problem.

Insert **Figure 12** here

Phosphorus can react electrochemically with sodium to form Na$_3$P at an attractive potential, possessing a theoretical specific capacity of 2596 mAh g^{-1}. Cui and co-workers designed a sandwiched nanostructure comprising few-layer phosphorene alternating with graphene sheets

(**Figure 12**).[29] The phosphorene sheets, with an increased interlayer distance, offer a short and effective diffusion path for sodium ions. The hybrid materials show an extremely high capacity of 2440 mAh g^{-1} at 50 mA g^{-1} with a capacity retention of 83% after 100 cycles. The high capacity is revealed by *in situ* transmission electron microscopy and *ex situ* X-ray diffraction techniques, indicating a dual mechanism of intercalation of sodium ions along the x axis of the phosphorene layers followed by the formation of a Na$_3$P alloy. It is concluded that the graphene sheets not only act as a mechanical backbone and an electrical conductor, but also serve as an elastic buffer space for accommodating the anisotropic expansion upon cycling operation. Besides phosphorene, other layered materials like metal sulfides and TMDs have also been combined with conductive matrix (e.g., RGO/graphene/conductive carbon) for SIBs.[178-188] For instance, Qu *et al.* designed a SnS$_2$-RGO nanocomposites using a facile hydrothermal route from a mixture of tin (IV) chloride, thioacetamide (TAA) and graphene oxide (GO).[179] The as-made electrode showed a high charge specific capacity (630 mAh g^{-1} at 0.2 A g^{-1}), good rate performance (544 mAh g^{-1} at 2 A g^{-1}) and long cycle-life (500 mAh g^{-1} at 1 A g^{-1} for 400 cycles). The good performance is attributed to the increased interlayer spacing of SnS$_2$, which could better accommodate the volume change in Na-Sn insertion and de-insertions, and also the improved conductivity owing to the presence of RGO. Shen and coworkers reported a novel synergistic Ni$_3$S$_2$-MoS$_2$ core-shell nanofiber superstructure on three dimensional nickel/graphene foam using a one- step polyvinylpyrrolidone-assisted hydrothermal reaction.[184] The as-fabricated hierarchical nanofibers can provide homogeneous atomic heterointerface with porous hierarchical structure, resulting in a high specific capacity (568 mAh g^{-1} at 0.2 A g^{-1}), an excellent rate capability (283 mAh g^{-1} at 5 A g^{-1}) as well as a good long-term cycle stability (207 mAh g^{-1} is retained after 400 cycles at 5 A g^{-1}), as an anode electrode for SIBs.

Owing to sodium's higher mass/atomic radius and more positive redox potential, SIBs show a lower energy density than LIBs. In particular, for the anodes of SIBs, the main issues include

large polarization and rapid capacity fading. Coulombic efficiency of each cycle still needs to be improved, probably due to the insufficient passivation in aprotic polar solvents when compared with LIBs. Moreover, SIBs still suffer from safety hazard because of the usage of organic electrolytes. Instead, using solid state electrolytes is expected to address the problem.

Insert **Table 3** here

4.3 Other types of batteries

Besides for LIBs and SIBs, GAs also hold potential applications in other kinds of batteries, such as Li-S,[189-192] Mg,[193] zinc−air/nickel,[194] Li-air batteries,[195, 196] *etc*. For a typical Li-S battery, it consists of a lithium anode, a sulfur cathode, and an electrolyte in between. During discharging, lithium is oxidized at the anode yielding lithium ions and electrons, and sulphur is reduced to lithium sulphide at the cathode. Backward reactions happen during charging.[197] Nazar and co-workers demonstrated a metallic Co_9S_8 material with an interconnected graphene-like nano-architecture which exhibits both metallic conductivity and hierarchical porosity, and the sheets were used as a cathode for Li-S batteries.[189] High discharge capacities of 1130, 890, 895, and 863 mAh g^{-1} were obtained at C/20, C/2, 1C and 2C rates, respectively. An ultralow capacity-fading rate of 0.045% per cycle over 1500 cycles was achieved. Sheets of oxygenated carbon nitrides[190] and MXenes[191] were also employed as electrodes in Li-S batteries, and both showed high electrochemical performance. Lee *et al*. reported $NiO/Ni(OH)_2$ nanoflakes as the active electrode material for a hybrid zinc−air/nickel battery.[194] The hybrid battery shows a remarkably high power density (volumetric, 14 000 W L^{-1}; gravimetric, 2700 W kg^{-1}), an energy density of 980 Wh kg^{-1}, and an excellent charge rate capability up to 10 times faster than the rate of discharge without any capacity and voltage degradations. Li-air batteries are also interesting energy storage systems due to their high specific energy, based on oxidation of lithium at the anode and reduction of oxygen at the cathode to induce a current flow. Salehi-Khojin and co-workers presented a cathode material using MoS_2 sheets combined with an ionic liquid, which was employed as an

effective co-catalyst for discharge and charge in a Li−O$_2$ battery.[195] CV measurements show excellent catalytic performance for both oxygen reduction and evolution reactions compared to Au and Pt catalysts. The co-catalyst also performs a high round-trip efficiency (∼85%) for the first cycle, which drops slightly to ∼80% after 50 cycles. All these studies open the door for further development of new type of advanced battery systems with high power and energy density.

5. Summary and Outlooks

The continuously growing interest in graphene related materials is reminiscent of the first decade of gold-rush on graphene. The broadest diversity of available GAs featuring well-distinct physical and chemical properties offers potential for breakthroughs in energy applications, and in particular for the development of high performance energy storage devices. In this review, we have summarized the recent developments on the use of GAs as electrode materials for electrochemical energy storage devices, such as supercapacitors and batteries. Although the progress in this highly dynamic field is quite impressive, the use of GAs in energy storage devices is still in its infancy. Presently their performance in energy storage devices is still low and needs to be drastically improved to target the goals of scalable applications and a promising market foreground. In particular, their inferior high rate performance and cycling stability hinder the implementation in real devices. Developing electrolyte/electrode systems that are efficient, stable, and cost-effective is still highly demanded.

Currently, either two- or three-electrode configurations are used to measure the performance of supercapacitors. However, it is known that, under lower current conditions, three-electrode configurations exhibit higher values of capacitance than two-electrode based architectures.[3, 198] In order to properly and fairly compare the results within literature, supercapacitors

integrating GAs should be characterized by using and comparing the results obtained with both two- and three-electrode configurations.[199] In order to further improve the performance of supercapacitors, it is essential to gain a better understanding on the dominant factors contributing to the capacitance. As for batteries, tremendous research efforts are still required on the design and study of new GAs and their hybrids as components for electrodes featuring a higher storage capacity, an improved columbic efficiency and a longer cycling life. For LIBs, there is still debate regarding to the actual lithiation reaction sequence during charging/discharging processes. For SIBs, low capacity and poor rate capability of existing anodes are the bottlenecks for future developments. Also, when one wants to compare the capacity from one material to another, a particular attention should be paid to the potential window, electrolytes, and composition of electrodes, charge/discharge efficiency as well as volumetric and areal capacities, all of which are largely overlooked/neglected. Recently, some efforts have already been made to design hybrid energy storage devices such as lithium/sodium-ion hybrid capacitors,[200, 201] which are expected to bridge the gap between LIBs and supercapacitors, possessing both high energy and power density.

The practical application of energy storage devices will depend critically on the preparation of novel functional layered materials with the advantages of low cost, high efficiency, large scale, and outstanding properties. Among the various methods proposed, *top-down* liquid-phase exfoliation and *bottom-up* wet chemical synthesis in liquid mediums are the most promising approaches to meet these requirements. Despite numerous efforts on the synthesis of a wide range of GAs, there is still a lack of reliable mass production methods to control their thicknesses (e.g., with a high percentage of single-layer sheets or well-defined numbers of layers on a large scale) and sizes to keep the morphology more homogeneously. Thus, new preparation strategies are highly and urgently demanded to produce high quality other 2D materials in a controlled way. The rational design of unique nanostructures holds the potential to solve the issues encountered during the electrochemical processes, thus may dramatically

increase the capacity and cycle life of energy storage devices. Increase of the specific surface area and optimization of the pore sizes and pore size distribution of GAs can be achieved by developing hierarchically porous nanostructures. The interfacial interactions between GAs and conductive fillers should be optimized by taking full advantage of the synergistic effects between the individual components, in order to minimize volume changes during charging/discharging. An emerging direction for GAs relies on designing new nanostructures, such as sandwiched multilayers and 3D hybrid structures with tuneable compositions/interlayer distances, for energy-related applications.

Although the excellent electrochemical properties of GAs have been revealed and studied, much needs to be done on the exploitation of these emerging properties for harnessing the device performance. Towards this end, a great effort should be devoted to unravelling the structure–electrochemical property relationships, which will be key for the design of novel electrode materials with superior performance. Major step forward in layered materials application in energy storage can be foreseen only when a fundamental understanding on the structures of electrodes, the electrode/electrolyte interfaces, and charge-storage mechanisms is attained, requiring both experimental and theoretical contributions.[202] Furthermore, the influence of defects on the electrochemical properties of layered materials needs to be systematically studied. Increasing the operating voltage is a useful way to improve the overall electrochemical performance (e.g., gravimetric energy density and power density) by choosing a suitable electrolyte with a high operating voltage window (organic electrolytes or ionic liquids).

When dealing with the design of graphene related materials for energy storage, it is key to find solutions that combine reasonable costs with acceptable performance. In other words, specific capacity, energy density, power density, life, cost, and safety, all need to be taken into serious consideration and should be well-balanced. Technically, light-weight, flexible energy storage systems that combine both outstanding electrochemical and mechanical (e.g., bending/

stretching) performance will boost the development and commercialization of next generation

flexible electronics. From the practical point of view, there is still a large technical gap

existing between laboratory research and industrial manufacturing. Therefore, a closer

collaboration between the communities of academy and industry is needed to solve the

encountered issues jointly, such as a low packing density and a strong tendency of

aggregation during processing for GAs, and accommodation of large volume changes during

charge/discharge cycles. Despite these big challenges to be tacked, the future of GAs in

energy storage devices is still bright. With the rapid progress of intense research on these

unique materials from both academy and industry, it is reasonable to expect that large-scale,

low-cost preparation of nanostructured GAs with *ad-hoc* electrochemical performance could

be realized for practical applications in the near future.

Received: ((will be filled in by the editorial staff))
Revised: ((will be filled in by the editorial staff))
Published online: ((will be filled in by the editorial staff))

[1]   Y. Gogotsi, P. Simon, *Science* **2011**, *334*, 917.
[2]   P. Simon, Y. Gogotsi, *Nat. Mater.* **2008**, *7*, 845.
[3]   M. D. Stoller, R. S. Ruoff, *Energy Environ. Sci.* **2010**, *3*, 1294.
[4]   F. Bonaccorso, L. Colombo, G. Yu, M. Stoller, V. Tozzini, A. C. Ferrari, R. S. Ruoff, V. Pellegrini, *Science* **2015**, *347*, 1246501.
[5]   D. Larcher, J. M. Tarascon, *Nat. Chem.* **2015**, *7*, 19.
[6]   Y. Huang, J. Liang, Y. Chen, *Small* **2012**, *8*, 1805.
[7]   A. C. Ferrari, F. Bonaccorso, V. Fal'ko, K. S. Novoselov, S. Roche, P. Boggild, S. Borini, F. H. Koppens, V. Palermo, N. Pugno, J. A. Garrido, R. Sordan, A. Bianco, L. Ballerini, M. Prato, E. Lidorikis, J. Kivioja, C. Marinelli, T. Ryhanen, A. Morpurgo, J. N. Coleman, V. Nicolosi, L. Colombo, A. Fert, M. Garcia-Hernandez, A. Bachtold, G. F. Schneider, F. Guinea, C. Dekker, M. Barbone, Z. Sun, C. Galiotis, A. N. Grigorenko, G. Konstantatos, A. Kis, M. Katsnelson, L. Vandersypen, A. Loiseau, V. Morandi, D. Neumaier, E. Treossi, V. Pellegrini, M. Polini, A. Tredicucci, G. M. Williams, B. H. Hong, J. H. Ahn, J. M. Kim, H. Zirath, B. J. van Wees, H. van der Zant, L. Occhipinti, A. Di Matteo, I. A. Kinloch, T. Seyller, E. Quesnel, X. Feng, K. Teo, N. Rupesinghe, P. Hakonen, S. R. Neil, Q. Tannock, T. Lofwander, J. Kinaret, *Nanoscale* **2015**, *7*, 4598.
[8]   X. Y. Zhang, L. L. Hou, P. Samorì, *Nat. Commun.* **2016**, *7*, 11128.
[9]   W. Feng, W. Luo, Y. Feng, *Nanoscale* **2012**, *4*, 6118.
[10]   X. Wan, Y. Huang, Y. Chen, *Acc. Chem. Res.* **2012**, *45*, 598.
[11]   C. N. R. Rao, H. S. S. Ramakrishna Matte, U. Maitra, *Angew. Chem. Int. Ed.* **2013**, *52*, 13162.
[12]   Y. Sun, S. Gao, F. Lei, C. Xiao, Y. Xie, *Acc. Chem. Res.* **2015**, *48*, 3.
[13]   S. L. Li, K. Tsukagoshi, E. Orgiu, P. Samorì, *Chem. Soc. Rev.* **2016**, *45*, 118.
[14]   X. Y. Zhang, E. H. Huisman, M. Gurram, W. R. Browne, B. J. van Wees, B. L. Feringa, *Small* **2014**, *10*, 1735.
[15]   H. Wang, H. Feng, J. Li, *Small* **2014**, *10*, 2165.
[16]   H. Li, Y. Shi, M.-H. Chiu, L.-J. Li, *Nano Energy* **2015**, *18*, 293.
[17]   R. Mas-Balleste, C. Gomez-Navarro, J. Gomez-Herrero, F. Zamora, *Nanoscale* **2011**, *3*, 20.
[18]   K. F. Mak, C. Lee, J. Hone, J. Shan, T. F. Heinz, *Phys. Rev. Lett.* **2010**, *105*, 136805.
[19]   Z. Yu, Z.-Y. Ong, Y. Pan, Y. Cui, R. Xin, Y. Shi, B. Wang, Y. Wu, T. Chen, Y.-W. Zhang, G. Zhang, X. Wang, *Adv. Mater.* **2016**, *28*, 547.
[20]   Y.-K. Hsu, Y.-C. Chen, Y.-G. Lin, L.-C. Chen, K.-H. Chen, *J. Mater. Chem.* **2012**, *22*, 2733.
[21]   H. Liu, A. T. Neal, Z. Zhu, Z. Luo, X. Xu, D. Tomanek, P. D. Ye, *ACS Nano* **2014**, *8*, 4033.
[22]   L. Li, Y. Yu, G. J. Ye, Q. Ge, X. Ou, H. Wu, D. Feng, X. H. Chen, Y. Zhang, *Nat. Nanotechnol.* **2014**, *9*, 372.
[23]   J.-C. Lei, X. Zhang, Z. Zhou, *Front. Phys.* **2015**, *10*, 276.
[24]   A. Miranda, J. Halim, M. W. Barsoum, A. Lorke, *Appl. Phys. Lett.* **2016**, *108*, 033102.
[25]   L. Matthes, O. Pulci, F. Bechstedt, *J. Phys.: Condens. Matter* **2013**, *25*, 395305.
[26]   L. Tao, E. Cinquanta, D. Chiappe, C. Grazianetti, M. Fanciulli, M. Dubey, A. Molle, D. Akinwande, *Nat. Nanotechnol.* **2015**, *10*, 227.
[27]   Y. Peng, Z. Meng, C. Zhong, J. Lu, W. Yu, Y. Jia, Y. Qian, *Chem. Lett.* **2001**, *30*, 772.
[28]   Z. Jia, J. Wang, Y. Wang, B. Li, B. Wang, T. Qi, X. Wang, *J. Mater. Sci. Technol.* **2016**, *32*, 147.
[29]   J. Sun, H. W. Lee, M. Pasta, H. Yuan, G. Zheng, Y. Sun, Y. Li, Y. Cui, *Nat. Nanotechnol.* **2015**, *10*, 980.
[30]   M. Naguib, J. Come, B. Dyatkin, V. Presser, P.-L. Taberna, P. Simon, M. W. Barsoum, Y. Gogotsi, *Electrochem. Commun.* **2012**, *16*, 61.

[31]   X. Chia, A. Y. S. Eng, A. Ambrosi, S. M. Tan, M. Pumera, *Chem. Rev.* **2015**, *115*, 11941.

[32]   M. Chhowalla, H. S. Shin, G. Eda, L. J. Li, K. P. Loh, H. Zhang, *Nat. Chem.* **2013**, *5*, 263.

[33]   R. Lv, J. A. Robinson, R. E. Schaak, D. Sun, Y. Sun, T. E. Mallouk, M. Terrones, *Acc. Chem. Res.* **2015**, *48*, 56.

[34]   V. Nicolosi, M. Chhowalla, M. G. Kanatzidis, M. S. Strano, J. N. Coleman, *Science* **2013**, *340*, 1226419.

[35]   Q. H. Wang, K. Kalantar-Zadeh, A. Kis, J. N. Coleman, M. S. Strano, *Nat. Nanotechnol.* **2012**, *7*, 699.

[36]   M. Xu, T. Liang, M. Shi, H. Chen, *Chem. Rev.* **2013**, *113*, 3766.

[37]   H. Zhang, *ACS Nano* **2015**, *9*, 9451.

[38]   G. Eda, H. Yamaguchi, D. Voiry, T. Fujita, M. Chen, M. Chhowalla, *Nano Lett.* **2011**, *11*, 5111.

[39]   J. N. Coleman, M. Lotya, A. O'Neill, S. D. Bergin, P. J. King, U. Khan, K. Young, A. Gaucher, S. De, R. J. Smith, I. V. Shvets, S. K. Arora, G. Stanton, H. Y. Kim, K. Lee, G. T. Kim, G. S. Duesberg, T. Hallam, J. J. Boland, J. J. Wang, J. F. Donegan, J. C. Grunlan, G. Moriarty, A. Shmeliov, R. J. Nicholls, J. M. Perkins, E. M. Grieveson, K. Theuwissen, D. W. McComb, P. D. Nellist, V. Nicolosi, *Science* **2011**, *331*, 568.

[40]   H. Li, J. Wu, Z. Yin, H. Zhang, *Acc. Chem. Res.* **2014**, *47*, 1067.

[41]   M. Yi, Z. Shen, *J. Mater. Chem. A* **2015**, *3*, 11700.

[42]   J. Cai, P. Ruffieux, R. Jaafar, M. Bieri, T. Braun, S. Blankenburg, M. Muoth, A. P. Seitsonen, M. Saleh, X. Feng, K. Müllen, R. Fasel, *Nature* **2010**, *466*, 470.

[43]   D. Lembke, S. Bertolazzi, A. Kis, *Acc. Chem. Res.* **2015**, *48*, 100.

[44]   X. Y. Zhang, A. C. Coleman, N. Katsonis, W. R. Browne, B. J. van Wees, B. L. Feringa, *Chem. Commun.* **2010**, *46*, 7539.

[45]   X. Y. Zhang, L. L. Hou, A. Cnossen, A. C. Coleman, O. Ivashenko, P. Rudolf, B. J. van Wees, W. R. Browne, B. L. Feringa, *Chem. Eur. J.* **2011**, *17*, 8957.

[46]   A. Ciesieslki, P. Samorì, *Adv. Mater.* **2016**, DOI: 10.1002/adma.201505371.

[47]   X. Y. Zhang, W. R. Browne, B. L. Feringa, *RSC Adv.* **2012**, *2*, 12173.

[48]   K. Parvez, Z. S. Wu, R. Li, X. Liu, R. Graf, X. Feng, K. Müllen, *J. Am. Chem. Soc.* **2014**, *136*, 6083.

[49]   N. Liu, P. Kim, J. H. Kim, J. H. Ye, S. Kim, C. J. Lee, *ACS Nano* **2014**, *8*, 6902.

[50]   Z. Zeng, T. Sun, J. Zhu, X. Huang, Z. Yin, G. Lu, Z. Fan, Q. Yan, H. H. Hng, H. Zhang, *Angew. Chem. Int. Ed.* **2012**, *51*, 9052.

[51]   S. Yang, M. R. Lohe, K. Müllen, X. Feng, *Adv. Mater.* **2016**, DOI: 10.1002/adma.201505326.

[52]   Z. Y. Xia, S. Pezzini, E. Treossi, G. Giambastiani, F. Corticelli, V. Morandi, A. Zanelli, V. Bellani, V. Palermo, *Adv. Funct. Mater.* **2013**, *23*, 4684.

[53]   X. Fan, P. Xu, D. Zhou, Y. Sun, Y. C. Li, M. A. Nguyen, M. Terrones, T. E. Mallouk, *Nano Lett.* **2015**, *15*, 5956.

[54]   J. C. Shaw, H. Zhou, Y. Chen, N. O. Weiss, Y. Liu, Y. Huang, X. Duan, *Nano Res.* **2015**, *7*, 511.

[55]   D. Kong, H. Wang, J. J. Cha, M. Pasta, K. J. Koski, J. Yao, Y. Cui, *Nano Lett.* **2013**, *13*, 1341.

[56]   Y. Zhan, Z. Liu, S. Najmaei, P. M. Ajayan, J. Lou, *Small* **2012**, *8*, 966.

[57]   Z. Sun, T. Liao, Y. Dou, S. M. Hwang, M. S. Park, L. Jiang, J. H. Kim, S. X. Dou, *Nat. Commun.* **2014**, *5*, 3813.

[58]   L. L. Zhang, X. S. Zhao, *Chem. Soc. Rev.* **2009**, *38*, 2520.

[59]   G. Wang, L. Zhang, J. Zhang, *Chem. Soc. Rev.* **2012**, *41*, 797.

[60]   L. Dai, D. W. Chang, J. B. Baek, W. Lu, *Small* **2012**, *8*, 1130.

[61]   Y. Zhai, Y. Dou, D. Zhao, P. F. Fulvio, R. T. Mayes, S. Dai, *Adv. Mater.* **2011**, *23*, 4828.

[62]   K. Hong, M. Cho, S. O. Kim, *ACS Appl. Mater. Interfaces* **2015**, *7*, 1899.

[63]   D. Feng, Y. Lv, Z. Wu, Y. Dou, L. Han, Z. Sun, Y. Xia, G. Zheng, D. Zhao, *J. Am. Chem. Soc.* **2011**, *133*, 15148.

[64]   H. He, L. Shi, Y. Fang, X. Li, Q. Song, L. Zhi, *Small* **2014**, *10*, 4671.

[65]   D. N. Futaba, K. Hata, T. Yamada, T. Hiraoka, Y. Hayamizu, Y. Kakudate, O. Tanaike, H. Hatori, M. Yumura, S. Iijima, *Nat. Mater.* **2006**, *5*, 987.

[66]   C. Liu, Z. Yu, D. Neff, A. Zhamu, B. Z. Jang, *Nano Lett.* **2010**, *10*, 4863.

[67]   J. Chmiola, C. Largeot, P. L. Taberna, P. Simon, Y. Gogotsi, *Science* **2010**, *328*, 480.

[68]   E. G. da Silveira Firmiano, A. C. Rabelo, C. J. Dalmaschio, A. N. Pinheiro, E. C. Pereira, W. H. Schreiner, E. R. Leite, *Adv. Energy Mater.* **2014**, *4*, 1301380.

[69]   H. Ji, C. Liu, T. Wang, J. Chen, Z. Mao, J. Zhao, W. Hou, G. Yang, *Small* **2015**, *11*, 6480.

[70]   M. Acerce, D. Voiry, M. Chhowalla, *Nat. Nanotechnol.* **2015**, *10*, 313.

[71]   M. A. Bissett, I. A. Kinloch, R. A. W. Dryfe, *ACS Appl. Mater. Interfaces* **2015**, *7*, 17388.

[72]   Y. Yang, H. Fei, G. Ruan, C. Xiang, J. M. Tour, *Adv. Mater.* **2014**, *26*, 8163.

[73]   J. M. Soon, K. P. Loh, *Electrochem. Solid-State Lett.* **2007**, *10*, A250.

[74]   J. Feng, X. Sun, C. Wu, L. Peng, C. Lin, S. Hu, J. Yang, Y. Xie, *J. Am. Chem. Soc.* **2011**, *133*, 17832.

[75]   L. Pan, G. Yu, D. Zhai, H. R. Lee, W. Zhao, N. Liu, H. Wang, B. C. Tee, Y. Shi, Y. Cui, Z. Bao, *Proc. Natl. Acad. Sci.* **2012**, *109*, 9287.

[76]   Q. Yang, Z. Lu, X. Sun, J. Liu, *Sci. Rep.* **2013**, *3*, 3537.

[77]   Y. Zhang, Y. Liu, J. Chen, Q. Guo, T. Wang, H. Pang, *Sci. Rep.* **2014**, *4*, 5687.

[78]   S. Gao, Y. Sun, F. Lei, L. Liang, J. Liu, W. Bi, B. Pan, Y. Xie, *Angew. Chem. Int. Ed.* **2014**, *53*, 12789.

[79]   H. Li, Y. Gao, C. Wang, G. Yang, *Adv. Energy Mater.* **2015**, *5*, 1401767.

[80]   M. Ghidiu, M. R. Lukatskaya, M.-Q. Zhao, Y. Gogotsi, M. W. Barsoum, *Nature* **2014**, *516*, 78.

[81]   M. R. Lukatskaya, S.-M. Bak, X. Yu, X.-Q. Yang, M. W. Barsoum, Y. Gogotsi, *Adv. Energy Mater.* **2015**, *5*, 1500589.

[82]   M. Boota, B. Anasori, C. Voigt, M. Q. Zhao, M. W. Barsoum, Y. Gogotsi, *Adv. Mater.* **2016**, *28*, 1517.

[83]   Z. Ling, C. E. Ren, M.-Q. Zhao, J. Yang, J. M. Giammarco, J. Qiu, M. W. Barsoum, Y. Gogotsi, *Proc. Natl. Acad. Sci.* **2014**, *111*, 16676.

[84]   J. Yan, Z. Fan, W. Sun, G. Ning, T. Wei, Q. Zhang, R. Zhang, L. Zhi, F. Wei, *Adv. Funct. Mater.* **2012**, *22*, 2632.

[85]   J. Chang, M. Jin, F. Yao, T. H. Kim, V. T. Le, H. Yue, F. Gunes, B. Li, A. Ghosh, S. Xie, Y. H. Lee, *Adv. Funct. Mater.* **2013**, *23*, 5074.

[86]   G. Sun, J. Liu, X. Zhang, X. Wang, H. Li, Y. Yu, W. Huang, H. Zhang, P. Chen, *Angew. Chem. Int. Ed.* **2014**, *53*, 12576.

[87]   F. Grote, Z. Y. Yu, J. L. Wang, S. H. Yu, Y. Lei, *Small* **2015**, *11*, 4666.

[88]   M. Q. Zhao, C. E. Ren, Z. Ling, M. R. Lukatskaya, C. Zhang, K. L. Van Aken, M. W. Barsoum, Y. Gogotsi, *Adv. Mater.* **2015**, *27*, 339.

[89]   T. Zhu, H. B. Wu, Y. Wang, R. Xu, X. W. Lou, *Adv. Energy Mater.* **2012**, *2*, 1497.

[90]   J. Zhao, J. Chen, S. Xu, M. Shao, Q. Zhang, F. Wei, J. Ma, M. Wei, D. G. Evans, X. Duan, *Adv. Funct. Mater.* **2014**, *24*, 2938.

[91]   N. Yu, H. Yin, W. Zhang, Y. Liu, Z. Tang, M.-Q. Zhu, *Adv. Energy Mater.* **2016**, *6*, 1501458.

[92]   J. Zhang, J. Fu, J. Zhang, H. Ma, Y. He, F. Li, E. Xie, D. Xue, H. Zhang, Y. Peng, *Small* **2014**, *10*, 2618.

[93]   P. Tang, L. Han, L. Zhang, S. Wang, W. Feng, G. Xu, L. Zhang, *ChemElectroChem* **2015**, *2*, 949.

[94]   H. Tang, J. Wang, H. Yin, H. Zhao, D. Wang, Z. Tang, *Adv. Mater.* **2015**, *27*, 1117.

[95]   J. Zhu, W. Sun, D. Yang, Y. Zhang, H. H. Hoon, H. Zhang, Q. Yan, *Small* **2015**, *11*, 4123.

[96]   J. Zhao, S. Xu, K. Tschulik, R. G. Compton, M. Wei, D. O'Hare, D. G. Evans, X. Duan, *Adv. Funct. Mater.* **2015**, *25*, 2745.

[97]   S. Peng, L. Li, H. B. Wu, S. Madhavi, X. W. Lou, *Adv. Energy Mater.* **2015**, *5*, 1401172.

[98]   J. Ji, L. L. Zhang, H. Ji, Y. Li, X. Zhao, X. Bai, X. Fan, F. Zhang, R. S. Ruoff, *ACS Nano* **2013**, *7*, 6237.

[99]   J. Chen, J. Xu, S. Zhou, N. Zhao, C.-P. Wong, *Nano Energy* **2016**, *21*, 145.

[100]   K. M. Hercule, Q. Wei, O. K. Asare, L. Qu, A. M. Khan, M. Yan, C. Du, W. Chen, L. Mai, *Adv. Energy Mater.* **2015**, *5*, 1500060.

[101]   J.-X. Feng, S.-H. Ye, A.-L. Wang, X.-F. Lu, Y.-X. Tong, G.-R. Li, *Adv. Funct. Mater.* **2014**, *24*, 7093.

[102]   X. Wang, C. Yan, A. Sumboja, J. Yan, P. S. Lee, *Adv. Energy Mater.* **2014**, *4*, 1301240.

[103]   Y. Tang, Y. Zhang, W. Li, B. Ma, X. Chen, *Chem. Soc. Rev.* **2015**, *44*, 5926.

[104]   J. B. Goodenough, Y. Kim, *Chem. Mater.* **2010**, *22*, 587.

[105]   G. Wang, X. Shen, J. Yao, J. Park, *Carbon* **2009**, *47*, 2049.

[106]   M. Liang, L. Zhi, *J. Mater. Chem.* **2009**, *19*, 5871.

[107]   Y. J. Lee, Y. Lee, D. Oh, T. Chen, G. Ceder, A. M. Belcher, *Nano Lett.* **2010**, *10*, 2433.

[108]   P. Poizot, S. Laruelle, S. Grugeon, L. Dupont, J. M. Tarascon, *Nature* **2000**, *407*, 496.

[109]   M. V. Reddy, G. V. Subba Rao, B. V. Chowdari, *Chem. Rev.* **2013**, *113*, 5364.

[110]   K. Cao, L. Jiao, H. Liu, Y. Liu, Y. Wang, Z. Guo, H. Yuan, *Adv. Energy Mater.* **2015**, *5*, 1401421.

[111]   J. Zhu, Z. Yin, D. Yang, T. Sun, H. Yu, H. E. Hoster, H. H. Hng, H. Zhang, Q. Yan, *Energy Environ. Sci.* **2013**, *6*, 987.

[112]   Y. Li, J. Yao, E. Uchaker, J. Yang, Y. Huang, M. Zhang, G. Cao, *Adv. Energy Mater.* **2013**, *3*, 1171.

[113]   M. Liu, C. Yan, Y. Zhang, *Sci. Rep.* **2015**, *5*, 8326.

[114]   J. S. Chen, Y. L. Tan, C. M. Li, Y. L. Cheah, D. Luan, S. Madhavi, F. Y. Boey, L. A. Archer, X. W. Lou, *J. Am. Chem. Soc.* **2010**, *132*, 6124.

[115]   H. Hu, L. Yu, X. Gao, Z. Lin, X. W. Lou, *Energy Environ. Sci.* **2015**, *8*, 1480.

[116]   Q. Wu, J. Xu, X. Yang, F. Lu, S. He, J. Yang, H. J. Fan, M. Wu, *Adv. Energy Mater.* **2015**, *5*, 1401756.

[117]   G. Yang, H. Cui, G. Yang, C. Wang, *ACS Nano* **2014**, *8*, 4474.

[118]   D. Rangappa, K. D. Murukanahally, T. Tomai, A. Unemoto, I. Honma, *Nano Lett.* **2012**, *12*, 1146.

[119]   T. Liu, Y. Feng, Y. Duan, S. Cui, L. Lin, J. Hu, H. Guo, Z. Zhuo, J. Zheng, Y. Lin, W. Yang, K. Amine, F. Pan, *Nano Energy* **2015**, *18*, 187.

[120]   H. Wang, S. Liu, Y. Ren, W. Wang, A. Tang, *Energy Environ. Sci.* **2012**, *5*, 6173.

[121]   S. Jin, G. Yang, H. Song, H. Cui, C. Wang, *ACS Appl. Mater. Interfaces* **2015**, *7*, 24932.

[122]   L. Sun, T. Su, L. Xu, M. Liu, H.-B. Du, *Chem. Commun.* **2016**, *52*, 4341.

[123]   Y.-S. Hu, R. Demir-Cakan, M.-M. Titirici, J.-O. Müller, R. Schlögl, M. Antonietti, J. Maier, *Angew. Chem. Int. Ed.* **2008**, *47*, 1645.

[124]   H. Liu, D. Su, R. Zhou, B. Sun, G. Wang, S. Z. Qiao, *Adv. Energy Mater.* **2012**, *2*, 970.

[125]   Y. Chen, B. Song, X. Tang, L. Lu, J. Xue, *Small* **2014**, *10*, 1536.

[126]   S. Qin, W. Lei, D. Liu, Y. Chen, *J. Mater. Chem. A* **2016**, *4*, 1440.

[127]   L. Luo, B. Zhao, B. Xiang, C.-M. Wang, *ACS Nano* **2016**, *10*, 1249.

[128]   Y. Zhang, X. Rui, Y. Tang, Y. Liu, J. Wei, S. Chen, W. R. Leow, W. Li, Y. Liu, J. Deng, B. Ma, Q. Yan, X. Chen, *Adv. Energy Mater.* **2016**, 1502409.

[129]   J. Luo, X. Tao, J. Zhang, Y. Xia, H. Huang, L. Zhang, Y. Gan, C. Liang, W. Zhang, *ACS Nano* **2016**, *10*, 2491.

[130]   M. Naguib, J. Halim, J. Lu, K. M. Cook, L. Hultman, Y. Gogotsi, M. W. Barsoum, *J. Am. Chem. Soc.* **2013**, *135*, 15966.

[131]   Y. Dou, J. Xu, B. Ruan, Q. Liu, Y. Pan, Z. Sun, S. X. Dou, *Adv. Energy Mater.* **2016**, 1501835.

[132]   V. Etacheri, J. E. Yourey, B. M. Bartlett, *ACS Nano* **2014**, *8*, 1491.

[133]   C. Chen, X. Hu, Y. Jiang, Z. Yang, P. Hu, Y. Huang, *Chem. Eur. J.* **2014**, *20*, 1383.

[134]   G. Zhou, D. W. Wang, L. C. Yin, N. Li, F. Li, H. M. Cheng, *ACS Nano* **2012**, *6*, 3214.

[135]   P. Xiong, L. Peng, D. Chen, Y. Zhao, X. Wang, G. Yu, *Nano Energy* **2015**, *12*, 816.

[136]   G. Gao, H. B. Wu, B. Dong, S. Ding, X. W. Lou, *Adv. Sci.* **2015**, *2*, 1400014.

[137]   G. Gao, H. B. Wu, X. W. Lou, *Adv. Energy Mater.* **2014**, *4*, 1400422.

[138]   S. M. Hao, J. Qu, J. Yang, C. X. Gui, Q. Q. Wang, Q. J. Li, X. Li, Z. Z. Yu, *Chem. Eur. J.* **2016**, *22*, 3397.

[139]   C. S. Rout, B. H. Kim, X. Xu, J. Yang, H. Y. Jeong, D. Odkhuu, N. Park, J. Cho, H. S. Shin, *J. Am. Chem. Soc.* **2013**, *135*, 8720.

[140]   L. Ma, J. Ye, W. Chen, D. Chen, J. Yang Lee, *Nano Energy* **2014**, *10*, 144.

[141]   G. Huang, T. Chen, W. Chen, Z. Wang, K. Chang, L. Ma, F. Huang, D. Chen, J. Y. Lee, *Small* **2013**, *9*, 3693.

[142]   R. Wang, C. Xu, J. Sun, Y. Liu, L. Gao, H. Yao, C. Lin, *Nano Energy* **2014**, *8*, 183.

[143]   X. Cao, Y. Shi, W. Shi, X. Rui, Q. Yan, J. Kong, H. Zhang, *Small* **2013**, *9*, 3433.

[144]   J. Wang, J. Liu, D. Chao, J. Yan, J. Lin, Z. X. Shen, *Adv. Mater.* **2014**, *26*, 7162.

[145]   Z. Yu, J. Song, M. L. Gordin, R. Yi, D. Tang, D. Wang, *Adv. Sci.* **2015**, *2*, 21400020.

[146]   L. Chen, G. Zhou, Z. Liu, X. Ma, J. Chen, Z. Zhang, X. Ma, F. Li, H. M. Cheng, W. Ren, *Adv. Mater.* **2016**, *28*, 510.

[147]   G. Huang, H. Liu, S. Wang, X. Yang, B. Liu, H. Chen, M. Xu, *J. Mater. Chem. A* **2015**, *3*, 24128.

[148]   Z. X. Huang, Y. Wang, J. I. Wong, H. Y. Yang, *2D Mater.* **2015**, *2*, 024010.

[149]   Y. Zhang, H. Wang, Z. Luo, H. T. Tan, B. Li, S. Sun, Z. Li, Y. Zong, Z. J. Xu, Y. Yang, K. A. Khor, Q. Yan, *Adv. Energy Mater.* **2016**, 1600453.

[150]   K. Chang, D. Geng, X. Li, J. Yang, Y. Tang, M. Cai, R. Li, X. Sun, *Adv. Energy Mater.* **2013**, *3*, 839.

[151]   Y. Tang, D. Wu, Y. Mai, H. Pan, J. Cao, C. Yang, F. Zhang, X. Feng, *Nanoscale* **2014**, *6*, 14679.

[152]   X. Wang, G. Li, M. H. Seo, F. M. Hassan, M. A. Hoque, Z. Chen, *Adv. Energy Mater.* **2015**, *5*, 1501106.

[153]   J. Zhu, K. Sakaushi, G. Clavel, M. Shalom, M. Antonietti, T. P. Fellinger, *J. Am. Chem. Soc.* **2015**, *137*, 5480.

[154]   Q. Qu, F. Qian, S. Yang, T. Gao, W. Liu, J. Shao, H. Zheng, *ACS Appl. Mater. Interfaces* **2016**, *8*, 1398.

[155]   J.-Z. Wang, L. Lu, M. Lotya, J. N. Coleman, S.-L. Chou, H.-K. Liu, A. I. Minett, J. Chen, *Adv. Energy Mater.* **2013**, *3*, 798.

[156]   J. Li, Y. Hou, X. Gao, D. Guan, Y. Xie, J. Chen, C. Yuan, *Nano Energy* **2015**, *16*, 10.

[157]   S. Ding, J. S. Chen, X. W. Lou, *Adv. Funct. Mater.* **2011**, *21*, 4120.

[158]   O. Mashtalir, M. R. Lukatskaya, M. Q. Zhao, M. W. Barsoum, Y. Gogotsi, *Adv. Mater.* **2015**, *27*, 3501.

29

[159]   J. Ni, Y. Zhao, L. Li, L. Mai, *Nano Energy* **2015**, *11*, 129.

[160]   X. Rui, X. Zhao, Z. Lu, H. Tan, D. Sim, H. H. Hng, R. Yazami, T. M. Lim, Q. Yan, *ACS Nano* **2013**, *7*, 5637.

[161]   Q. An, F. Xiong, Q. Wei, J. Sheng, L. He, D. Ma, Y. Yao, L. Mai, *Adv. Energy Mater.* **2015**, *5*, 1401963.

[162]   J. Ryu, D. Hong, S. Choi, S. Park, *ACS Nano* **2016**, *10*, 2843.

[163]   N. Li, G. Zhou, F. Li, L. Wen, H.-M. Cheng, *Adv. Funct. Mater.* **2013**, *23*, 5429.

[164]   H. Jiang, D. Ren, H. Wang, Y. Hu, S. Guo, H. Yuan, P. Hu, L. Zhang, C. Li, *Adv. Mater.* **2015**, *27*, 3687.

[165]   Y. Liu, M. Zhu, D. Chen, *J. Mater. Chem. A* **2015**, *3*, 11857.

[166]   Y. Zhang, Y. Wang, J. Yang, W. Shi, H. Yang, W. Huang, X. Dong, *2D Mater.* **2016**, *3*, 024001.

[167]   G. Gao, S. Lu, B. Dong, Z. Zhang, Y. Zheng, S. Ding, *J. Mater. Chem. A* **2015**, *3*, 4716.

[168]   Z. Wan, J. Shao, J. Yun, H. Zheng, T. Gao, M. Shen, Q. Qu, H. Zheng, *Small* **2014**, *10*, 4975.

[169]   F. Zhou, S. Xin, H. W. Liang, L. T. Song, S. H. Yu, *Angew. Chem. Int. Ed.* **2014**, *53*, 11552.

[170]   X. Y. Yu, H. Hu, Y. Wang, H. Chen, X. W. Lou, *Angew. Chem. Int. Ed.* **2015**, *54*, 7395.

[171]   J. Deng, C. Yan, L. Yang, S. Baunack, S. Oswald, H. Wendrock, Y. Mei, O. G. Schmidt, *ACS Nano* **2013**, *7*, 6948.

[172]   L. Yang, S. Wang, J. Mao, J. Deng, Q. Gao, Y. Tang, O. G. Schmidt, *Adv. Mater.* **2013**, *25*, 1180.

[173]   S. Guo, H. Yu, Z. Jian, P. Liu, Y. Zhu, X. Guo, M. Chen, M. Ishida, H. Zhou, *ChemSusChem* **2014**, *7*, 2115.

[174]   S. Guo, P. Liu, H. Yu, Y. Zhu, M. Chen, M. Ishida, H. Zhou, *Angew. Chem. Int. Ed.* **2015**, *54*, 5894.

[175]   W. Sun, X. Rui, D. Yang, Z. Sun, B. Li, W. Zhang, Y. Zong, S. Madhavi, S. Dou, Q. Yan, *ACS Nano* **2015**, *9*, 11371.

[176]   D. Su, S. Dou, G. Wang, *Adv. Energy Mater.* **2015**, *5*, 1401205.

[177]   B. Ahmed, D. H. Anjum, M. N. Hedhili, H. N. Alshareef, *Small* **2015**, *11*, 4341.

[178]   T. Zhou, W. K. Pang, C. Zhang, J. Yang, Z. Chen, H. K. Liu, Z. Guo, *ACS Nano* **2014**, *8*, 8323.

[179]   B. Qu, C. Ma, G. Ji, C. Xu, J. Xu, Y. S. Meng, T. Wang, J. Y. Lee, *Adv. Mater.* **2014**, *26*, 3854.

[180]   Y. Zhang, P. Zhu, L. Huang, J. Xie, S. Zhang, G. Cao, X. Zhao, *Adv. Funct. Mater.* **2015**, *25*, 481.

[181]   S. H. Choi, Y. N. Ko, J.-K. Lee, Y. C. Kang, *Adv. Funct. Mater.* **2015**, *25*, 1780.

[182]   X. Xie, Z. Ao, D. Su, J. Zhang, G. Wang, *Adv. Funct. Mater.* **2015**, *25*, 1393.

[183]   L. David, R. Bhandavat, G. Singh, *ACS Nano* **2014**, *8*, 1759.

[184]   J. Wang, J. Liu, H. Yang, D. Chao, J. Yan, S. V. Savilov, J. Lin, Z. X. Shen, *Nano Energy* **2016**, *20*, 1.

[185]   J. Wang, C. Luo, T. Gao, A. Langrock, A. C. Mignerey, C. Wang, *Small* **2015**, *11*, 473.

[186]   X. Xie, T. Makaryan, M. Zhao, K. L. Van Aken, Y. Gogotsi, G. Wang, *Adv. Energy Mater.* **2016**, *6*, 1502161.

[187]   Y. Lu, Q. Zhao, N. Zhang, K. Lei, F. Li, J. Chen, *Adv. Funct. Mater.* **2016**, *26*, 911.

[188]   Z.-T. Shi, W. Kang, J. Xu, Y.-W. Sun, M. Jiang, T.-W. Ng, H.-T. Xue, D. Y. W. Yu, W. Zhang, C.-S. Lee, *Nano Energy* **2016**, *22*, 27.

[189]   Q. Pang, D. Kundu, L. F. Nazar, *Mater. Horiz.* **2016**, *3*, 130.

[190]   J. Liu, W. Li, L. Duan, X. Li, L. Ji, Z. Geng, K. Huang, L. Lu, L. Zhou, Z. Liu, W. Chen, L. Liu, S. Feng, Y. Zhang, *Nano Lett.* **2015**, *15*, 5137.

[191]   X. Liang, A. Garsuch, L. F. Nazar, *Angew. Chem. Int. Ed.* **2015**, *54*, 3907.

[192]   Z. W. Seh, J. H. Yu, W. Li, P.-C. Hsu, H. Wang, Y. Sun, H. Yao, Q. Zhang, Y. Cui, *Nat. Commun.* **2014**, *5*, 5017.

[193]   Y. Liang, R. Feng, S. Yang, H. Ma, J. Liang, J. Chen, *Adv. Mater.* **2011**, *23*, 640.

[194]   D. U. Lee, J. Fu, M. G. Park, H. Liu, A. Ghorbani Kashkooli, Z. Chen, *Nano Lett.* **2016**, *16*, 1794.

[195]   M. Asadi, B. Kumar, C. Liu, P. Phillips, P. Yasaei, A. Behranginia, P. Zapol, R. F. Klie, L. A. Curtiss, A. Salehi-Khojin, *ACS Nano* **2016**, *10*, 2167.

[196]   P. Zhang, X. Lu, Y. Huang, J. Deng, L. Zhang, F. Ding, Z. Su, G. Wei, O. G. Schmidt, *J. Mater. Chem. A* **2015**, *3*, 14562.

[197]   A. Manthiram, Y. Fu, S.-H. Chung, C. Zu, Y.-S. Su, *Chem. Rev.* **2014**, *114*, 11751.

[198]   V. Khomenko, E. Frackowiak, F. Béguin, *Electrochim. Acta* **2005**, *50*, 2499.

[199]   X. Y. Zhang, A. Ciesielski, F. Richard, P. Chen, E. A. Prasetyanto, L. De Cola, P. Samori, *Small* **2016**, *12*, 1044.

[200]   Y. Ma, H. Chang, M. Zhang, Y. Chen, *Adv. Mater.* **2015**, *27*, 5296.

[201]   X. Wang, S. Kajiyama, H. Iinuma, E. Hosono, S. Oro, I. Moriguchi, M. Okubo, A. Yamada, *Nat. Commun.* **2015**, *6*, 6544.

[202]   A. C. Forse, C. Merlet, J. M. Griffin, C. P. Grey, *J. Am. Chem. Soc.* **2016**, DOI: 10.1021/jacs.6b02115.

Author biographies and photographs

Dr. Xiaoyan Zhang obtained his PhD in December 2013, from Stratingh Institute for Chemistry and Zernike Institute for Advanced Materials, University of Groningen, the Netherlands. He is currently a postdoctoral researcher in the group of Professor Paolo Samorì at the Institut de Science et d'Ingénierie Supramoléculaires (ISIS) of the University of Strasbourg, France. His current research interest focuses on preparation, characterization and functionalization of 2D materials for functional nanocomposites and energy-related applications.

Paolo Samorì is Distinguished Professor and director of the Institut de Science et d'Ingénierie Supramoléculaires (ISIS) of the Université de Strasbourg (UdS). He is also Fellow of the Royal Society of Chemistry (FRSC), fellow of the European Academy of Sciences (EURASC), member of the Academia Europaea (MAE) and junior member of the Institut Universitaire de France (IUF). His research interests include layered materials, organic semiconductors, hierarchical self-assembly of hybrid architectures, supramolecular electronics, and the fabrication of organic- and graphene-based nanodevices. His work was awarded various prizes, including the Young Scientist Awards at E-MRS (1998) and MRS (2000), the IUPAC Prize for Young Chemists (2001), the "Vincenzo Caglioti" Award (2006) granted by the Accademia Nazionale dei Lincei (Italy), the ERC Starting Grant (2010) and the CNRS Silver Medal (2012).
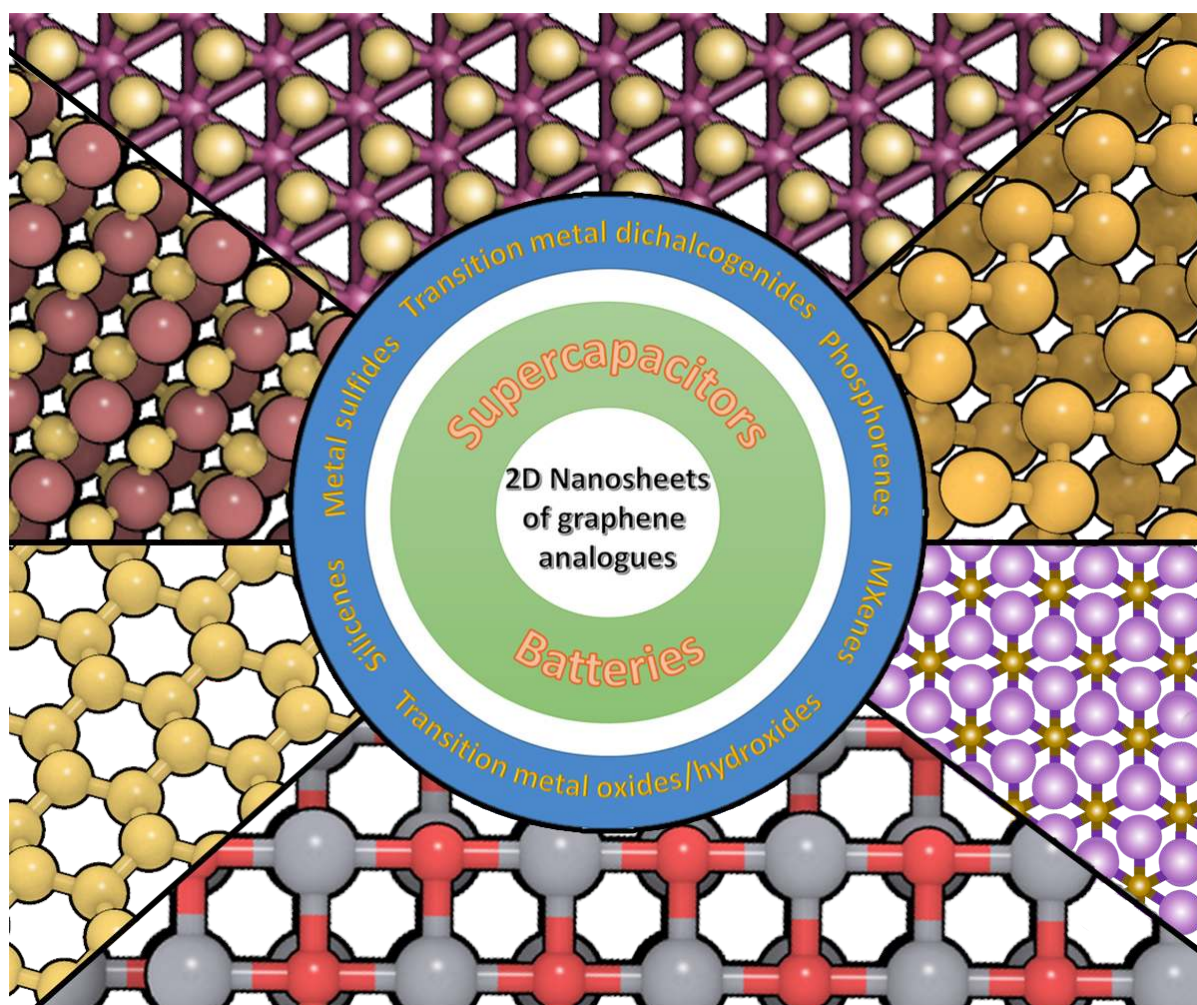
Figure 1. Typical 2D graphene analogues for energy storage and their structures.
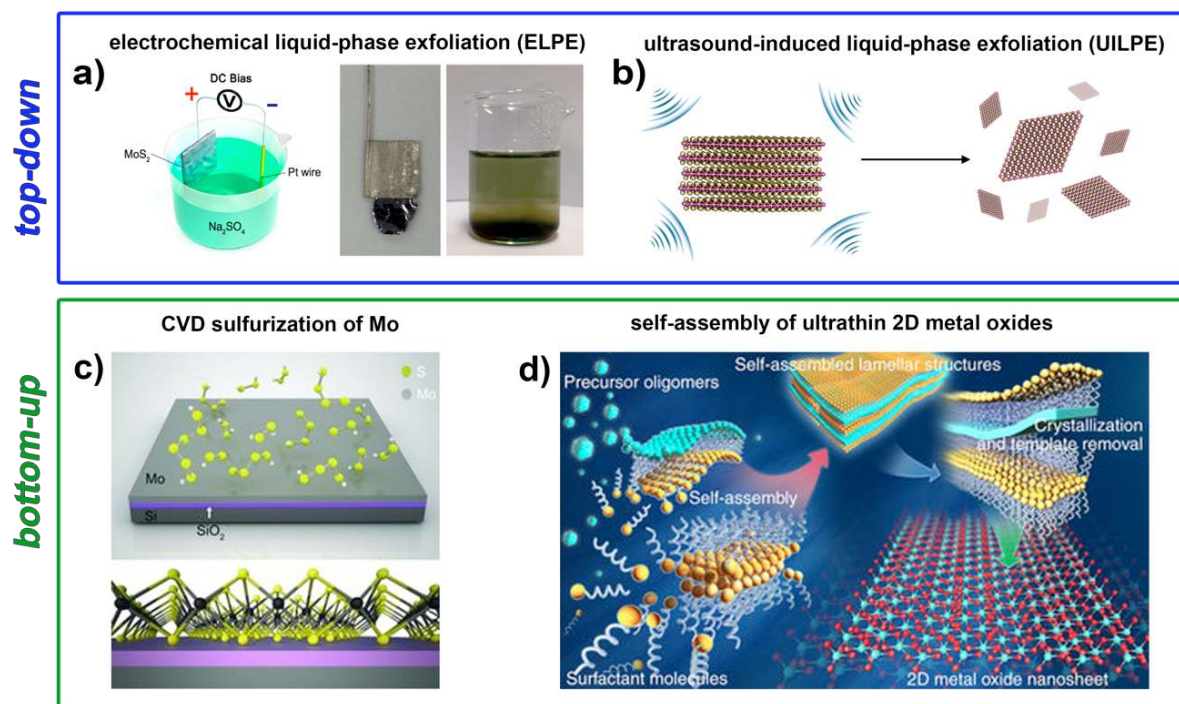
Figure 2. Schematic representation of *top-down* and *bottom-up* production methods of 2D materials. **a)** Schematic illustration of experimental setup for electrochemical liquid-phase exfoliation (ELPE) of bulk MoS_2 crystal (left); Photograph of a bulk MoS_2 crystal held by a Pt clamp before exfoliation (center); Exfoliated MoS_2 flakes suspended in a Na_2SO_4 electrolyte (right). Reproduced with permission from reference 49 (Copyright 2014 American Chemical Society). **b)** Scheme of ultrasound-induced liquid-phase exfoliation (UILPE) of MoS_2 crystal into individual sheets. **c)** CVD based process relying on the introduction of sulphur atoms on the Mo thin film that was pre-deposited on the SiO_2 substrate. Reproduced with permission from reference 56 (Copyright 2012 Wiley). **d)** Schematic shows the concept of molecular assembly of ultrathin 2D metal oxide sheets from liquid solutions, where metal oxide precursor oligomers are self-assembled into 2D metal oxide sheets with atomic thickness. Reproduced with permission from reference 57 (Copyright 2014 Nature Publishing Group).
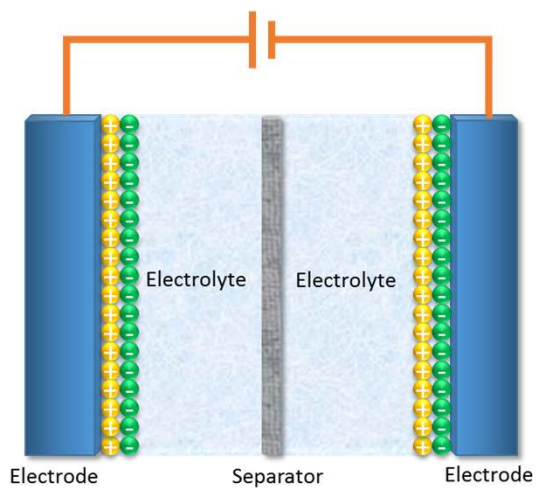
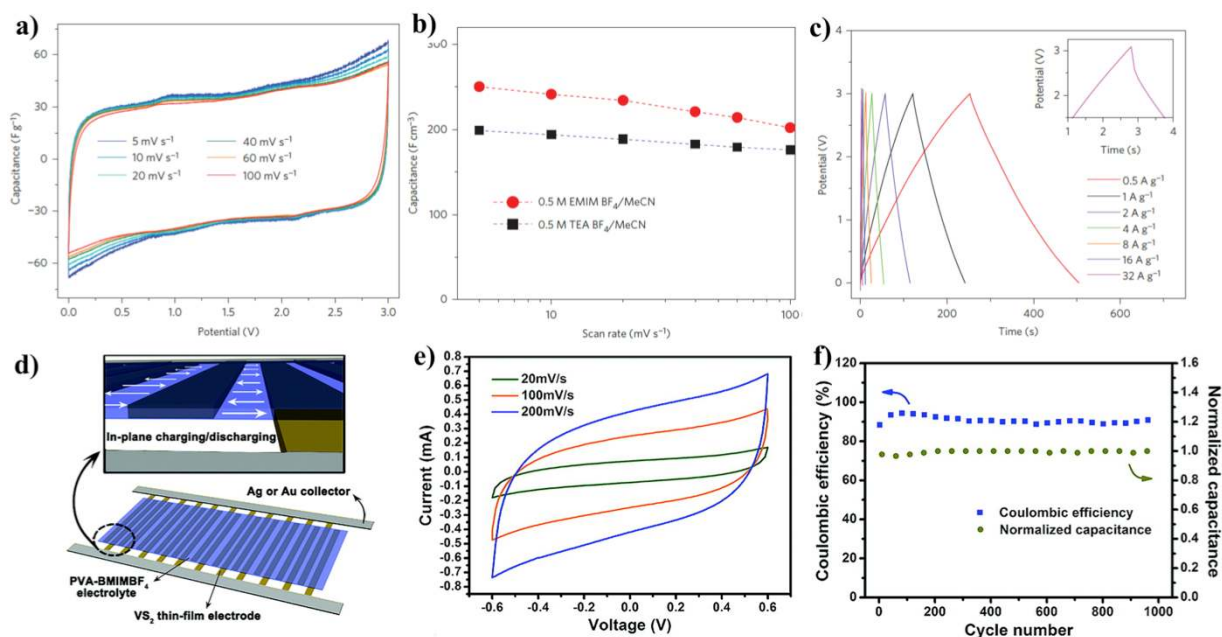**Figure 3.** Electrical double-layer capacitors (EDLCs) during charging.

Figure 4. Electrochemical characterization of metallic MoS_2 sheets for supercapacitors: **a)** CV curves in 1 M TEA BF_4/MeCN. **b)** Capacitance versus scan rate in TEA BF_4/MeCN and EMIM BF_4/MeCN electrolytes. **c)** Galvanostatic charge/discharge curves in TEA BF_4/MeCN at current rates from 0.5 $A\,g^{-1}$ to 32 $A\,g^{-1}$ (inset: Low internal resistance of the 1T MoS_2 electrodes in 1 M TEA BF_4/MeCN at a current density of 32 $A\,g^{-1}$). Figure 4a-c are reproduced from reference 70 (Copyright 2015 Nature Publishing Group). Electrochemical characterization of metallic VS_2 sheets for supercapacitors: **d)** Schematic illustration of the in-plane configuration of the as-fabricated supercapacitor using a VS_2 thin film electrode. **e)** CV curves at different scanning rates (20, 100, and 200 mV s^{-1}). **f)** Cycle performance of the supercapacitor, showing negligible degradations in the coulomb efficiency (left side y-axis) and specific capacitance (right side y-axis). Figure 4d-f are reproduced with permission from reference 74 (Copyright 2011 American Chemical Society).
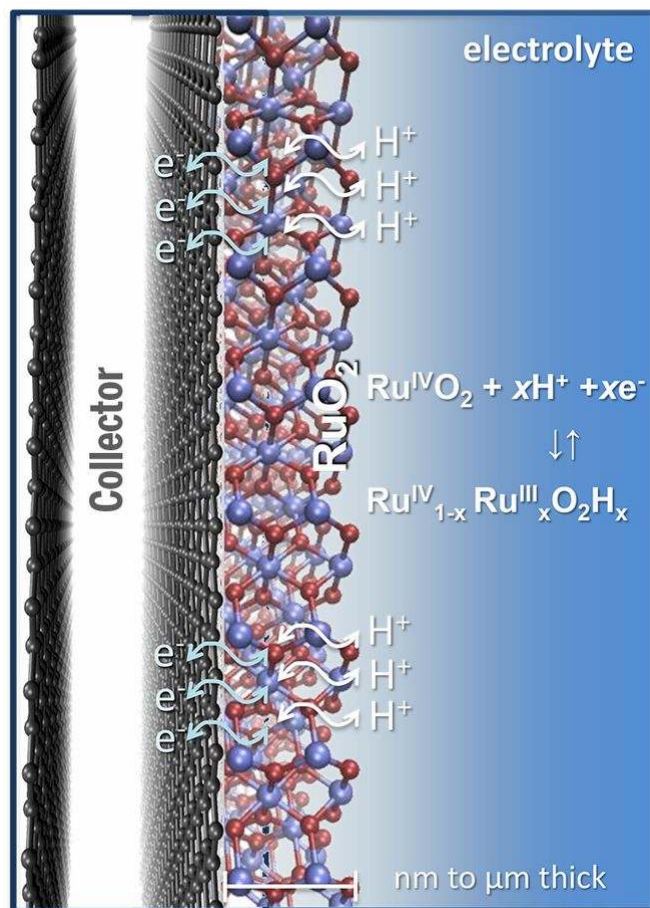
Figure 5. Charge transfer near the surface of the electrode for pseudocapacitors. Reproduced with permission from reference 4 (Copyright 2015 AAAS).
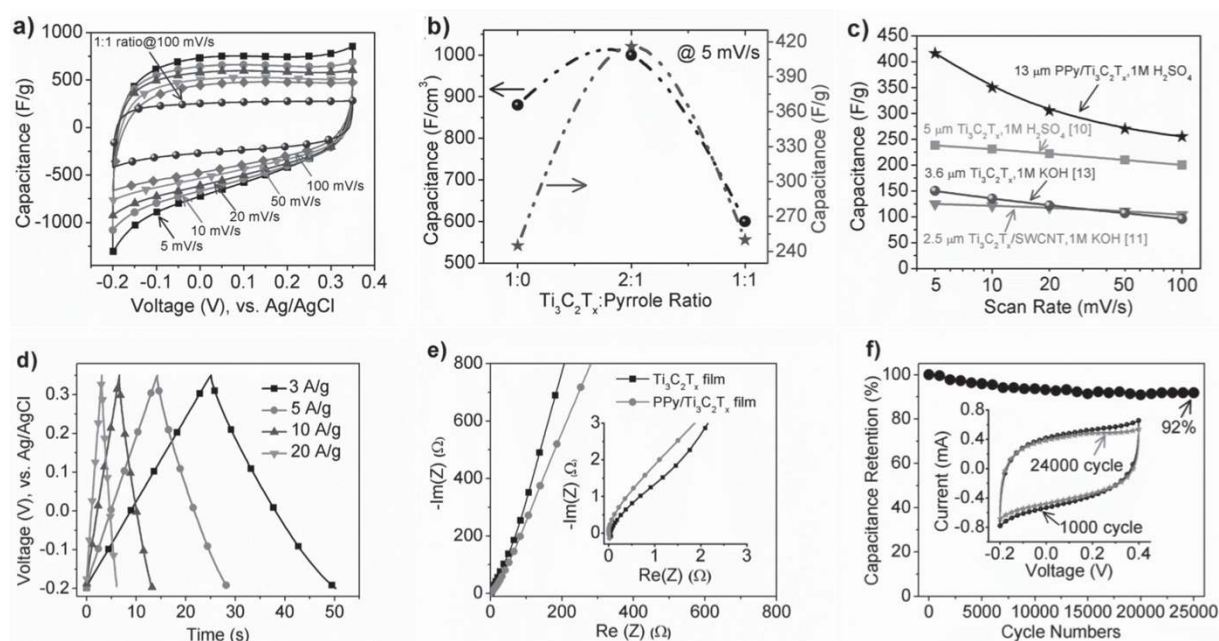
Figure 6. Electrochemical characterization of PPy/Ti$_3$C$_2$T$_x$ composites for supercapacitors: **a)** CV curves of PPy/Ti$_3$C$_2$T$_x$ (1:2) film at various scan rates. **b)** Effect of pyrrole loading on volumetric (left side y-axis) and gravemetric (right side y-axis) capacitance measured at 5 mV s^{-1}. **c)** Rate performance of tested compositions and comparisons of their capacitances with previously reported Ti$_3$C$_2$T$_x$ electrodes. **d)** Galvanostatic charge/discharge cycles of a PPy/Ti$_3$C$_2$T$_x$ (1:2) film at various current densities. **e)** Impedance spectra of pristine Ti$_3$C$_2$T$_x$ and PPy/Ti$_3$C$_2$T$_x$ (1:2) films. Inset: zoom-in of the high-frequency region. **f)** Cycle life performance showing high capacitance retention of the PPy/Ti$_3$C$_2$T$_x$ (1:2) film after 25000 cycles at 100 mV s^{-1}. Inset shows that the shape of the CV was retained after cycling, confirming the high electrochemical stability of the PPy confined between the MXene layers. Reproduced with permission from reference 82 (Copyright 2016 Wiley).

Figure 7. Cellulose paper (CP)-based asymmetrical, flexible thin film supercapacitors. **a)** Scheme of the assembled device using graphite/Ni/Co_2NiO_4 sheets-CP as positive electrode and graphite/Ni/active carbon-CP as negative electrode. **b)** CV curves of the device under various bending states at 50 mV s^{-1}. **c)** Cycle performance of the device at different bending states for 20 000 cycles at 100 mV s^{-1} and 10 mA cm^{-2}. Reproduced with permission from reference 101 (Copyright 2014 Wiley).

Figure 8. 3D hierarchical porous α-Fe$_2$O$_3$ sheets for LIBs: **a)** Rate capabilities of binder-free electrodes. **b)** Rate capabilities of scraped layer electrodes. **c)** Electrochemical impedance spectra (EIS) of the fresh cells, with the inset showing the equivalent circuit used to interpret the data (Randles circuit: Rs–series resistance, CPE1–double layer capacitance, Rct–charge transfer resistance, and W1–Warburg impedance describing diffusion of ions). EIS was performed at an amplitude of 5 mV (0.1–100 kHz). Reproduced with permission from reference 110 (Copyright 2015 Wiley).

Figure 9. Electrochemical performances of the $Co_3V_2O_8$ sheets for LIBs. **a)** and **b)** Reversible charge/discharge capacities against cycle number for samples obtained at 1 min and 12 h at different current densities of 1 and 5 A g^{-1} in the voltage window of 0.01–2.5 V. **c)** and **d)** Corresponding charge/discharge profiles in the first, 100th, 200th, 300th, 400th, and 500th cycles of the samples 1 min and 12 hrs at the current density of 5 A g^{-1}. **e)** Schematic illustration of electron-transfer pathways for two samples. **f)**. Corresponding Coulombic efficiencies. **g)** Rate performance of the $Co_3V_2O_8$ sheets obtained at 12 hrs. Reproduced with permission from reference 117 (Copyright 2014 American Chemical Society).

Figure 10. Electrochemical and microscopic characterization of MoS$_2$/S-doped RGO electrodes for LIBs. **a)** CV plots of a representative MoS$_2$/S-doped RGO composite electrode at a sweep rate of 0.1 mV s^{-1} between 3.0 and 0.005 V. The two peaks at 0.99 and 0.45 V for the initial cycle correspond to the Li$^+$ intercalation process forming Li$_x$MoS$_2$, and the further conversion to Mo embedded in Li$_2$S matrix, respectively. **b)** Galvanostatic charge/discharge curves of a composite electrode at a current densities of 0.1 A g^{-1} between 3.0 and 0.005 V. The low open circuit voltage (OCV) might be due to self-discharging. **c)** Comparison of cycling stability of MoS$_2$/S-doped RGO composites with pure MoS$_2$ and physically mixed MoS$_2$ and S-doped RGO at a current density of 0.1 A g^{-1}. **d)** Long-term cycling performance of MoS$_2$/S-doped RGO composites at a high current density of 10 A g^{-1} (inset: the Nyquist plot of the composite electrode at frequencies from 100 kHz to 0.01 Hz at different cycling status). **e)** high-magnification high angle annular dark field scanning transmission electron microscopy (HAADF-STEM) image of MoS$_2$/S-doped RGO composite after cycling test and the corresponding energy-dispersive X-ray spectroscopy (EDS) mapping of the elements C, Mo, and S. **f)** High-resolution TEM images of as-synthesized MoS$_2$/S-doped RGO composites after cycling test. Reproduced with permission from reference 152 (Copyright 2015 Wiley).

Figure 11. Electrochemical measurement of CNFs@MoS2 for LIBs. **a)** Galvanostatic discharge–charge (GDC) profiles. **b).** Cycling performance of CNFs@MoS$_2$ at 0.1 A g^{-1}. **c)** GDC profiles and **d)** cycling performance of CNFs@MoS$_2$ at different current densities. **e)** Long life cycling performance of CNFs@MoS$_2$ at 1 A g^{-1}. Reproduced with permission from reference 169 (Copyright 2014 Wiley).

Figure 12. Electrochemical measurement of the phosphorene–graphene anode for SIBs. **a)**. Reversible desodiation capacities for the first 100 galvanostatic cycles of various phosphorene–graphene electrodes with different carbon/phosphorus mole ratios (C/P) of 1.39, 2.07, 2.78 and 3.46, between 0.02 and 1.5 V at a current density of 0.05 A g^{-1}. **b)**. Galvanostatic discharge–charge curves of the phosphorene–graphene (48.3 wt% P) anode plotted for the first, second and 50th cycles. **c)**. Volumetric and mass capacities at different current densities (from 0.05 to 26 A g^{-1}). **d)**. Reversible desodiation capacity and Coulombic efficiency for the first 100 galvanostatic cycles of the phosphorene/graphene (48.3 wt% P) hybrid anode tested at different current densities. Reproduced with permission from reference 29 (Copyright 2015 Nature Publishing Group).

Table 1. Properties typical 2D graphene analogues.

Materials	Band gap (eV)	Mobility ($cm^2 V^{-1} s^{-1}$)	Surface area ($m^2 g^{-1}$)
MoS$_2$ (TMDs)	1.8 (Ref. 18)	148 (single-layer, 300 K, Ref. 19)	180–240 (hydrothermal, Ref. 27)
MnO$_2$ (TMOs)	2.1 (optical, Ref. 20)	–	257.5 (wet chemistry, Ref. 28)
Phosphorene	1.45 (Ref. 21)	1000 (few-layer, Ref. 22)	367 (liquid phase exfoliation, Ref. 29)
MXene	Metallic or narrow band gap semiconductor (Ref. 23)	0.7 ± 0.2 (Ref. 24)	23 (Ref. 30)
Silicene	1.9×10^{-3} (Ref. 25)	100 (RT, Ref. 26)	–

Table 2. Summary of supercapacitor performance of 2D graphene analogues.

Ref.	Electrodes	Electrolyte	Electrode configuration	Supercapacitor performance	Cycle performance
70	Metallic 1 T MoS_2	0.5 M H_2SO_4, Li_2SO_4, Na_2SO_4, K_2SO_4 KCl or KBr; 1M TEA BF_4 or EMIM BF_4 in acetonitrile	Three/Two	Volumetric capacitance (400 ~ 700 F cm^{-3})	>90% retained after 5000 cycles
74	Metallic VS_2	$BMIMBF_4$–PVA	Two	Capacitance (4760 μF cm^{-2})	No obvious degradation after 1000 cycles
76	Co_3O_4 (anode) activated carbon (cathode)	2 M KOH	Two/Three	Two-electrode: Capacitance (108 F g^{-1}) Energy density (134 Wh kg^{-1}); Three-electrode: Capacitance (1782 F g^{-1} at 1.8 A g^{-1})	Three-electrode: >90% retained after 2000 cycles at 30 mA cm^{-2}; Two-electrode: >80% retained after 800 cycles at 30 mA cm^{-2}
77	$Co_3V_2O_8$	3 M KOH	Three	Capacitance (739 F g^{-1} at 0.5 A g^{-1})	>95.3% retained after 2000 cycles 0.5 A g^{-1}
78	β-$Co(OH)_2$ (cathode) Nitrogen-doped graphene (anode)	PVA solid electrolyte (2 M KOH)	Two	Energy density (98.9 Wh kg^{-1}) Power density (17981 W kg^{-1})	93.2% retained after 10000 cycles 20 mV s^{-1}
84	Porous graphene (anode) $Ni(OH)_2$/graphene (cathode)	6 M KOH	Two	Capacitance (218.4 F g^{-1}) Energy density (77.8 Wh kg^{-1})	94.3% retained after 3000 cycles at 100 mV s^{-1}
85	RGO/MnO_2 (anode) RGO/MoO_3 (cathode)	1 M Na_2SO_4	Two	Capacitance (307 F g^{-1} at 0.2 A g^{-1}) Energy density (42.6 Wh kg^{-1}) Power density (276 W kg^{-1})	Capacitance increased after 1000 cycles at 50 mV s^{-1}
86	RGO/TMDs	PVA-H_2SO_4	Two	Volumetric capacitance (16.5 F cm^{-3} at 1 μA)	80% retained after 1000 cycles
87	$Co_{(1-x)}Ni_x(OH)_2$/RGO	1 M KOH	Three	Capacitance (1075, 1359 F g^{-1} at 100, 1 A g^{-1}, respectively)	72% retained after 7000 cycles at 20 A g^{-1}
88	MXene/CNTs	1 M $MgSO_4$	Three	Volumetric capacitance (350 F cm^{-3} at 5 A g^{-1})	No degradation after 10 000 cycles at 10 A g^{-1}
89	$CNT@Ni_3S_2$	2 M KOH	Three	Capacitance (514, 362 F g^{-1} at 4, 13.3 A g^{-1}, respectively	88% retained after 1500 cycles at 5.3 A g^{-1}
90	NiMn double hydroxide/CNT (anode) RGO/CNT (cathode)	Nafion/KOH	Two	Energy density (88.3 Wh kg^{-1}) Power density (850 W kg^{-1})	>94% retained after 1000 cycles at 10 A g^{-1}

91	MnO$_2$/Carbon fibers	1 M Na$_2$SO$_4$ PVA/LiCl	Three/Two	Capacitance (634.5 F g^{-1} at 2.5 A g^{-1}); Capacitance (87.1 F g^{-1} at 1.25 A g^{-1}) energy density (27.2 Wh kg^{-1}) power density (979.7 W kg^{-1})	Slight decrease after 3000 cycles at 20 A g^{-1}; 95.2% retained after 3000 cycles at 6.25 A g^{-1}
93	MnO$_2$@PEDOT @MnO$_2$	0.5 M Na$_2$SO$_4$	Two	Energy density (47.8 Wh kg^{-1}) Power density (180 W kg^{-1})	91.3% retained after 5000 cycles at 3 A g^{-1}
94	MoS$_2$/polypyrrole	1 M KCl	Two	Capacitance (695, 500 F g^{-1} at 0.5, 10 A g^{-1}, respectively) Energy density (83.3 Wh kg^{-1}) Power density (3332 W kg^{-1})	85% retained after 4000 cycles at 1 A g^{-1}
95	MoS$_2$/polyaninline	0.5 M H$_2$SO$_4$	Two	Capacitance (180 F g^{-1} at 50 A g^{-1}) Energy density (106 Wh kg^{-1}) Power density (106 kW kg^{-1})	91% retained after 4000 cycles at 10 A g^{-1}
82	MXene/polypyrrole	1 M H$_2$SO$_4$	Three	Volumetric capacitance (1000 F cm^{-3})	92% retained after 25000 cycles at 100 mV s^{-1}
97	NiMoO$_4$ on conductive substrates (Anode) activated carbon (cathode)	2 M KOH	Two	Energy density (60.9 Wh kg^{-1}) Power density (850 W kg^{-1})	85.7% retained after 10000 cycles at 5 A g^{-1}
98	Ni(OH)$_2$/ultrathin-graphite foam (Anode); Activated microwave exfoliated graphite oxide (Cathode)	6 M KOH	Two	Energy density (6.9 Wh kg^{-1}) Power density (44 kW kg^{-1})	63.2% retained after 10000 cycles at 5 A g^{-1}
99	FeOOH (anode) Co–Ni double hydroxides (cathod)	3 M KOH	Two	Energy density (86.4Wh kg^{-1}) Power density (11.6 kW kg^{-1})	92.3% retained after 3000 cycles at 100 mV s^{-1}
100	Li$_2$Co$_2$(MoO$_4$)$_3$ on conductive substrates	Several alkaline electrolytes	Three	Capacitance (1055, 700 F g^{-1} at 1, 50 A g^{-1}, respectively)	91% retained after 10000 cycles at 30 A g^{-1}
102	Nickel-cobalt-aluminum layered hydroxides	2 M NaOH	Three	Capacitance (1289, 738 F g^{-1} at 1, 30 A g^{-1}, respectively)	82.2% retained after 2000 cycles at 5 A g^{-1}

RGO–reduced graphene oxide; CNT–carbon nanotube

Table 3. Summary of battery performance of 2D graphene analogues.

Ref.	Electrodes	Electrolyte	Battery type	Battery performance	Cycle performance
110	α-Fe_2O_3 (anode) Home-made $LiFePO_4$ (cathode)	1 M $LiPF_6$ in a 1:1 mixture of ethylene carbonate and dimethyl carbonate	LIBs	Specific capacity (827.9 mAh g^{-1} at 2.01 A g^{-1})	Increased to 877.7 mAh g^{-1} after 1000 cycles at 2.01 A g^{-1}
112	V_2O_5	1 M $LiPF_6$ in a 1:1 (v/v) mixture of ethylene carbonate and dimethyl carbonate	LIBs	Specific capacity (219 mAh g^{-1} at 1 A g^{-1})	78% retained after 100 cycles at 0.5 A g^{-1}
113	Nb_2O_5	1 M $LiPF_6$ in a 1:1:1 mixture of ethylene carbonate/dimethyl carbonate/diethyl carbonate	LIBs	Specific capacity (90, 184 mAh g^{-1} at 1, 0.2 A g^{-1}, respectively)	77.8% retained after 200 cycles at 5 C
114	TiO_2	1 M $LiPF_6$ in a 1:1 mixture of ethylene carbonate and diethyl carbonate	LIBs	Specific capacity (224,192, 170 mAh g^{-1} at 0.5, 1, 5 C, respectively)	87.5% retained after 100 cycles at 1 C
115	TiO_2 (B)	1 M $LiPF_6$ in a 1:1 (v/v) mixture of ethylene carbonate and dimethyl carbonate	LIBs	Specific capacity (182, 202, 216 mAh g^{-1} at 5, 2, 1 C, respectively)	87.9% retained after 400 cycles at 5 C
116	Anatase/TiO_2-B	1 M $LiPF_6$ in a 1:1 (v/v) mixture of ethylene carbonate and dimethyl carbonate	LIBs	Specific capacity (221 mAh g^{-1} at 1.7 A g^{-1})	86% retained after 1000 cycles at 1.7 A g^{-1}
117	$Co_3V_2O_8$	1 M $LiPF_6$ in a 1:1 (v/v) mixture of ethylene carbonate and diethyl carbonate	LIBs	Specific capacity (525, 361 mAh g^{-1} at 5, 10 A g^{-1}, respectively)	1114 mAh g^{-1} is retained after 100 cycles at 1 A g^{-1}
119	$LiFePO_4$	1 M $LiPF_6$ in a 1:1:1 (v/v/v) mixture of ethylene chloride/ dimethyl chloride/diethyl chloride	LIBs	Specific capacity (107, 185 mAh g^{-1} at 20, 0.1 C, respectively)	97% retained after 400 cycles at 10 C
120	$Na_{1.08}V_3O_8$	1 M $LiPF_6$ in a 1:1 (v/v) mixture of ethylene carbonate and dimethyl carbonate	LIBs	Discharge capacity (200, 131.3, 109.9, 94.2, 72.5 mAh g^{-1} at 0.4, 10, 20, 30, 50 C, respectively)	No considerable capacity loss over 200 cycles at 1 A g^{-1}
125	Fe_3O_4 nanoparticles/MoS_2	1 M $LiPF_6$ in a 1:1:1 mixture of ethylene carbonate/dimethyl carbonate/diethyl carbonate	LIBs	Specific capacity (1033, 224 mAh g^{-1} at 2, 10 A g^{-1}, respectively)	Increased capacity after 510 cycles at 2 A g^{-1}
130	Nb_2CT_x or V_2CT_x	1 M $LiPF_6$ in a 1:1 (w/w) mixture of ethylene carbonate and diethyl carbonate	LIBs	Reversible capacity (170 and 260 mAh g^{-1} at 1 C for Nb_2CT_x and V_2CT_x,	110 and 125 mAh g^{-1} were obtained after 150 cycles at 10 C for Nb_2CT_x and V_2CT_x,

				respectively)	respectively
132	TiO$_2$–B/RGO	1 M LiPF$_6$ in a 1:1:1 mixture of ethylene carbonate/dimethyl carbonate/diethyl carbonate	LIBs	Specific capacity (275 mAh g^{-1} at 1 C)	80% retained after 1000 cycles at 40 C
133	TiO$_2$-B nanosheets/Anatase nanocrystals/RGO	1 M LiPF$_6$ in a 1:1 (v/v) mixture of ethylene carbonate and dimethyl carbonate	LIBs	Specific capacity (160, 154 mAh g^{-1} at 36, 72 C, respectively)	155 mAh g^{-1} is retained after 100 cycles at 36 C
135	ZnMn$_2$O$_4$/RGO (anode) LiFePO$_4$ (cathode)	1 M LiPF$_6$ in a 1:1 (v/v) mixture of ethylene carbonate and diethyl carbonate	LIBs	Specific capacity (122, 109, 90 mAh g^{-1} at 0.5, 1, 2 C, respectively)	No obvious decay after 100 cycles at 2, 5, 10 C
142	MoS$_2$/RGO	1 M LiPF$_6$ in a 1:1 (w/w) mixture of ethylene carbonate and dimethyl carbonate	LIBs	Specific capacity (598, 880, 994 mAh g^{-1} at 5, 1, 0.5 A g^{-1}, respectively)	100.6% retained after 1000 cycles at 1 A g^{-1}
143	MoS$_2$/graphene	1 M LiPF$_6$ in a 1:1 (v/v) mixture of ethylene carbonate and diethyl carbonate	LIBs	Specific capacity (10th cycle capability of 466 mAh g^{-1} at 4 A g^{-1})	566 mAh g^{-1} is retained after 50 cycles at 0.5 A g^{-1}
146	Black phosphorus/graphene	1 M LiPF$_6$ in a mixture of 1:1:1 (v/v/v) ethylene carbonate/dimethyl carbonate/ethylmethyl carbonate	LIBs	Specific capacity (920, 501, 141 mAh g^{-1} at 0.1, 0.5, 2.5 A g^{-1}, respectively)	80.2% retained after 500 cycles at 0.5 A g^{-1}
152	MoS$_2$/S-doped RGO	1 M LiPF$_6$ in a 1:1 (v/v) mixture of ethylene carbonate and dimethyl carbonate	LIBs	Specific capacity (1672, 915 mAh g^{-1} at 0.1, 10 A g^{-1}, respectively)	92.3% retained after 2000 cycles at 10 A g^{-1}
153	Metal carbide@N-doped carbon nanosheets	1 M LiPF$_6$ in a 1:1 mixture of ethylene carbonate and dimethyl carbonate	LIBs	Capacity (1010, 580, 495 mAh g^{-1} at 0.2, 0.5, 5 A g^{-1}, respectively)	Increased to 648 mAh g^{-1} after 680 cycles at 0.5 A g^{-1}
154	MoS$_2$/CNT	1 M LiPF$_6$ in a 1:1 (v/v) mixture of ethylene carbonate and dimethyl carbonate	LIBs	Specific capacity (610 mAh g^{-1} at 5 C)	>97% retained after 150 cycles at 1 C
156	MoS$_2$/CNT	1 M LiPF$_6$ in a 40:60 (v/v) mixture of ethylene carbonate and dimethyl carbonate	LIBs	Specific capacity (827.9 mAh g^{-1} at 2.01 A g^{-1})	96% retained after 425 cycles at 1 A g^{-1}
157	TiO$_2$/CNT SnO$_2$/CNT	1 M LiPF$_6$ in a 1:1 (w/w) mixture of ethylene carbonate and diethyl carbonate	LIBs	Specific capacity (320 mAh g^{-1} at 1 C for TiO$_2$/CNT; ~580 mAh g^{-1} for SnO$_2$/CNT at 0.4 A g^{-1})	93.8% retained after 120 cycles at 1 C for TiO$_2$/CNT; ~72.4% retained after 40 cycles at 0.4 A g^{-1} for SnO$_2$/CNT
158	Nb$_2$CT$_x$/CNT	1 M LiPF$_6$ in a 1:1 mixture of ethylene carbonate and diethyl	LIBs	Volumetric capacitance (325 F cm^{-3} at 5	Increased from 320 to 430 mAh g^{-1} after 300

		carbonate		mV s^{-1})	cycles at 2.5 C
159	MoO$_2$/C	1 M LiPF$_6$ in a 1:1 (v/v) mixture of ethylene carbonate and dimethyl carbonate	LIBs	Specific capacity (544 mAh g^{-1} at 10 A g^{-1})	Increased capacity after 100 cycles at 0.5 A g^{-1}
161	Na$_3$V$_2$(PO$_4$)$_3$/C	1 M LiPF$_6$ in a 1:1 (v/v) mixture of ethylene carbonate and dimethyl carbonate	LIBs	Specific capacity (230 mAh g^{-1} at 0.91 C)	83.6% retained after 5000 cycles at 9.1 C
162	Carbon-coated silicene	1.3 M LiPF$_6$ in a mixture of 3:7 (v/v) ethylene carbonate/diethyl carbonate with 10 wt% fluorinated ethylene carbonate	LIBs	Specific capacity (865 mAh g^{-1} at 1 A g^{-1})	92.3, 91.7% retained after 500 cycles at 0.5, 1 C, respectively
163	Nitrogen-doped carbon coated Li$_4$Ti$_5$O$_{12}$	1 M LiPF$_6$ in a 1:1 mixture of ethylene carbonate and dimethyl carbonate	LIBs	Specific capacity (170, 131 mAh g^{-1} at 1, 10 C, respectively)	No obvious deterioration over 100 cycles at 10 C
169	MoS$_2$/carbon nanofibers	1 M LiPF$_6$ in ethylene carbonate/dimethyl carbonate/diethyl carbonate (1:1:1 in wt%)	LIBs	Specific capacity (864 mAh g^{-1} at 5 A g^{-1})	Slightly decease after 300 cycles at 1 A g^{-1}
170	MoS$_2$/N-doped carbon nanoboxes	1 M LiPF$_6$ in a 1:1 (w/w) mixture of ethylene carbonate and diethyl carbonate	LIBs	Specific capacity (689, 531, 403 mAh g^{-1} at 2, 4, 8 A g^{-1}, respectively)	952 mAh g^{-1} is retained after 200 cycles at 0.4 A g^{-1}
174	Na$_{0.66}$Li$_{0.18}$Mn$_{0.71}$Ni$_{0.21}$Co$_{0.08}$O$_{2+\delta}$	1 M NaPF$_6$ in a 1:1 (v/v) mixture of ethylene carbonate and diethyl carbonate	SIBs	Discharge capacity (134 mAh g^{-1} at 1 C)	84% retainted after 50 cycles at 0.2 C and 75% retained after 150 cycles at 0.5 C
176	MoS$_2$	1 M NaClO$_4$ in a 1:1 (v/v) mixture of ethylene carbonate and propylene carbonate	SIBs	Specific capacity (530 mAh g^{-1} at 0.04 A g^{-1})	330, 305, 251 mAh g^{-1} is retained after 100 cycles at 0.08, 0.16, 0.32 A g^{-1}, respectively
29	Phosphorene-graphene	1 M NaPF$_6$ in a mixture of ethylene carbonate and diethyl carbonate with 10 % fluoroethylene carbonate	SIBs	Capacity (2440, 2320, 1450, 1200, 915, 645 mAh g^{-1} at 0.02, 0.08, 3, 4.6, 7.7, 10 C, respectively)	84% retained after 100 cycles at 3 C
178	SnS@RGO	1 M NaClO$_4$ in a 1:1 (v/v) mixture of ethylene carbonate and propylene carbonate with 5 wt% fluoroethylene carbonate	SIBs	Specific capacity (940 mAh g^{-1} at 0.03 A g^{-1})	492, 308 mAh g^{-1} is retained after 250 cycles at 0.81, 7.29 A g^{-1}, respectively
179	SnS$_2$/RGO	1 M NaClO$_4$ in a 1:1 (v/v) mixture of ethylene carbonate and diethyl carbonate	SIBs	Specific capacity (630, 544 mAh g^{-1} at 0.2, 2 A g^{-1}, respectively)	500 mAh g^{-1} is retained after 400 cycles at 1 A g^{-1}
181	MoS$_2$/RGO	1 M NaClO$_4$ in a 1:1 (v/v) mixture of ethylene carbonate and dimethyl	SIBs	Discharge capacity (385 mAh g^{-1} at 1.5	84% retained after 600 cycles

		carbonate with 5 wt% fluoroethylene carbonate		A g^{-1})	at 1.5 A g^{-1}
182	MoS$_2$/RGO	1 M NaClO$_4$ in a 1:1 (v/v) mixture of ethylene carbonate and propylene carbonate	SIBs	Specific capacity (352 mAh g^{-1} at 0.64 A g^{-1})	254, 227 mAh g^{-1} is retained after 300 cycles at 0.08, 0.32 A g^{-1}, respectively
184	MoS$_2$/Ni$_3$S$_2$@MoS$_2$ on 3D Ni/graphene foam	1 M NaPF$_6$ in a 1:1 (v/v) mixture of ethylene carbonate and diethyl carbonate with 3 vol% fluoroethylene carbonate	SIBs	Specific capacity (568, 283 mAh g^{-1} at 0.2, 5 A g^{-1}, respectively)	207 mAh g^{-1} is retained after 400 cycles at 5 A g^{-1}

RGO–reduced graphene oxide; CNT–carbon nanotube